Heliyon 10 (2024) e34295

Contents lists available at ScienceDirect

Heliyon

journal homepage: www.cell.com/heliyon

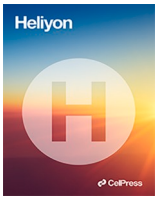

Research article

Identification of macrophage differentiation related genes and subtypes linking atherosclerosis plaque processing and metabolic syndrome via integrated bulk and single-cell sequence analysis

Da-Sheng Ning [a,b,c,*], Zi-Qing Zhou [a,b,c], Shu-Heng Zhou [a,b,c], Ji-Mei Chen [a,b,c,**]

[a] Guangdong Cardiovascular Institute, Guangdong Provincial People's Hospital (Guangdong Academy of Medical Sciences), Guangzhou 510080, PR China
[b] Department of Cardiovascular Surgery, Guangdong Provincial People's Hospital (Guangdong Academy of Medical Sciences), Southern Medical University, Guangzhou 510080, PR China
[c] Southern China Key Laboratory of Structural Heart Disease, Guangdong Provincial People's Hospital, Guangdong Academy of Medical Sciences, Guangzhou 510080, PR China

ARTICLE INFO

Keywords:
Atherosclerosis
Metabolic syndrome
Macrophage differentiation
Immune infiltration
Mechine learning
Single-cell RNA sequence analysis

ABSTRACT

Metabolic syndrome(MS) is a separate risk factor for the advancement of atherosclerosis(AS) plaque but mechanism behind this remains unclear. There may be a significant role for the immune system in this process. This study aims to identify potential diagnostic genes in MS patients at a higher risk of developing and progressing to AS. Datasets were retrevied from gene expression omnibus(GEO) database and differentially expressed genes were identified. Hub genes, immune cell dysregulation and AS subtypes were identified using a conbination of muliple bioinformatic analysis, machine learning and consensus clustering. Diagnostic value of hub genes was estimated using a nomogram and ROC analysis. Finally, enrichment analysis, competing endogenous RNA (ceRNA) network, single-cell RNA(scRNA) sequencing analysis and drug-protein interaction prediction was constructed to identify the functional roles, potential regulators and distribution for hub genes. Four hub genes and two macrophage-related subtypes were identified. Their strong diagnostic value was validated and functional process were identified. ScRNA analysis identified the macrophage differentiation regulation function of F13A1. CeRNA network and drug-protein binding modes revealed the potential therapeutic method. Four immune-correlated hub genes (F13A1, MMRN1, SLCO2A1 and ZNF521) were identified with their diagnostic value being assesed, which F13A1 was found strong correlated with macrophage differentiation and could be potential diagnostic and therapeutic marker for AS progression in MS patients.

1. Introduction

Atherosclerosis(AS) is a multi-factor derived disease that leading to the development of endothelial lesions, recruitment of leukocytes, deposition of oxidized lipids, accumulation of macrophages and foam cells, infiltration of smooth muscle cells, formation of

* Corresponding author. Guangdong Cardiovascular Institute, Guangdong Provincial People's Hospital (Guangdong Academy of Medical Sciences), Guangzhou 510080, PR China.
** Corresponding author.
E-mail addresses: dashengning@outlook.com (D.-S. Ning), chenjimei@gdph.org.cn (J.-M. Chen).

https://doi.org/10.1016/j.heliyon.2024.e34295
Received 13 December 2023; Received in revised form 28 June 2024; Accepted 8 July 2024
Available online 11 July 2024

plaques and thickening of artery walls [1]. The subsequent stenosis of artery lumen and rupture of AS plaques could result in cardiovascular and cerebrovascular incidents [2]. Several significant risk factors, including genetic factors, hypertension, hypercholesterolaemia, obesity, diabetes and smoking play pivotal roles in the process of plaque formation [3]. Despite extensive research efforts focusing on the pathogenesis and mechanism of AS, individualized prediction and prevention of AS plaque formation and progression remains a challenging endeavor.

Metabolic syndrome(MS) is a long-term non-infectious health issue characterized by abdominal obesity, hypertension, hyperlipidemia, impaired glucose metabolism and insulin resistance, which could give rise to a spectrum of pathologies, including pro-inflammatory states, pro-thrombotic tendencies, and oxidative stress [4–7]. MS has become a major issue in global public health concern due to its escalating prevalence and the severity of its complications, leading to worrisome trend of increased AS morbidity among younger individuals [8]. It is well recognized that hastens the process of AS plaque formation [9,10]. The inflammatory process linked to MS is thought to be crucial in both plaque development and subsequent clinical events [11]. However, owing to the subtle symptoms during the early stages of AS plaque progression, individuals with MS tend not to take their pathological condition seriously until cardiovascular complications become evident. Thus, it's imperative to explore a specific and sensitive tool for the early detection of AS, especially for the patients with MS who have higher risk and often possess limited awareness of their condition.

Due to the rapid progress of detection method such as proteomics and sequencing tools, there emerges an opportunity to identify novel candidate markers for disease prediction and prevention. Machine learning is progressively being employed to unearth biomarkers, elucidate underlying mechanisms, and pinpoint potential therapeutic targets within the realm of disease research.Limited research has been dedicated to potential prediction, diagnosis and prevention candidates specifically in MS patients who have an elevated risk of AS progression. Three AS plaque datasets and one MS dataset were acquired from the gene expression omnibus (GEO) database for this research. Differential expression genes(DEGs) was analyzed using the Limma algorithm, then crucial module genes were identified with weighted gene co-expression network analysis(WGCNA). Candidate genes were then identified using functional enrichment analysis, protein to protein interaction network, machine learning analysis, nomogram and receiver operating characteristic(ROC) analysis. Potential mechanisms and targets for prevention were finally predicted through single gene set enrichment analysis (sGSEA), the establishment of competing endogenous RNA (ceRNA) network, consensus clustering, drug-protein interaction modes and scRNA analysis.

2. Materials and methods

2.1. Mircoarray data

Raw datasets for AS advanced plaque and early intimae were obtained from patients (GSE28829, GSE97210 and GSE104140), as well as peripheral blood mononuclear cells(PBMCs) datasets (GSE181646) from metabolic syndrome(MS) patients via the GEO database (https://www.ncbi.nlm.nih.gov/geo) [12].

2.2. Data preprocessing and DEG screening

The probe name in the expression matrix files of GSE28829, GSE97210, GSE104140 and GSE181646 was annotated with the official gene symbol name using GPL570, GPL16956, GPL18573 and GPL30209. Then, GSE28829, GSE97210 and GSE104140 matrix were merged using R package "sva" to remove the batch effects. Normalization and DEGs screening were performed using the R package "Limma". Basically the mean and variance of each batch were estimated independently for each gene using the combat method, on the basis of the prior distribution of estimated parameters. Then we used counts matrix of merged datasets and converted the data to logs. The "Limma" R package utilized Bayesian techniques to calculate the conditional effect size of individual genes, with the p-value determined using a *t*-test.DEGs screening thresholds were set as $|\text{Log2 FC}| > 1$ for AS filtration or $|\text{Log2 FC}| > 1$ for MS filtration with a p-value <0.05.

2.3. Co-expression network construction by WGCNA

We utilized WGCNA to explore gene correlations. Firstly, the median absolute deviation(MAD) was calculated for every gene, and then 25 % of genes with the highest MAD were remained. Secondly, function of "goodSamplesGenes" was processed to screen the expression matrix, eliminating any genes and samples that did not meet the criteria. Thirdly, "soft" threshold power (β) derived by the similarity of co-expression was chosen to allocate the weights. Subsequently, a topological overlap measure was contrusted using anjacency for detecting gene module. In the fifth step, a gene dendrogram was created with a minimum gene module size set to $n = 30$. Finally, the similar modules were merged and the final modules were utilized for the further analysis.

2.4. Functional enrichment analysis

Genes were subjected to functional enrichment analysis using the Gene Ontology (GO) system and the Kyoto Encyclopedia of Genes and Genomes (KEGG) database, with the employing of R package "clusterProfiler" [13,14]. The visualization of enrichment analysis results was conducted via Bioinformatics platform(https://www.bioinformatics.com.cn). GO and KEGG analysis were conducted on DEGs for advanced AS, as well as on the intersection genes between DEGs and remarkable module of MS, along with the overlap of DEGs for AS and MS.

2.5. Machine learning

We utilized LASSO regression, RandomForest (RF), Gradient Boosting Machine (GBM), decision tree, Support Vector Machine with Recursive Feature Elimination (SVM-RFE), and Extreme Gradient Boosting (XGBoost) to pinpoint central genes linked to the advancement of AS plaques [15,16]. For LASSO regression, we utilized the R package "glmnet" and determined the optimal lambda, considering minimal lambda, with nlambda = 100 and alpha = 1. RandomForest analysis was processed using the "randomForest" R package. The datasets were split into training and validation sets using a 7:3 ratio, 5 nodesize and 500 decision ntrees were employed in the analysis with mtry = 3. We choose 10 fold for cross-validation with step = 0.9. In XGBoost analysis, we used the R package "xgboost" with the "xgbTree" method with max depth = 6, gamma = 0, subsample = 1 and eta = 0.3. SVM-RFE was executed using R packages "e1071" and "kernlab" and optimization parameters were selected through 10-fold cross-validation and halve.above = 30. We applied the GBM model with the R package "gbm" with shrinkage = 0.001, n.trees = 100 and interaction.depth = 1. Additionally, for decision tree analysis, the R package "rattle" was used with default parameter settings. The hub genes was identified through intersection results of all machine learning analysis.

2.6. Protein-protein interaction network construction

The protein-protein interaction (PPI) network was built using the STRING database (version 11.5; www.string-db.org). The minimal interaction score was set at 0.400 and the maximum first shell interactors was set at 10 [17]. The mediators of each hub gene were identified through PPI network.

2.7. Nomogram and receiver operating characteristic analysis

A nomogram was constructed to facilitate clinical diagnosis of the AS plaque process based on the candidate genes. The expression matrix counts data of GSE104140, GSE28829 and GSE97210 were converted to log and then were converted into risk scores based on multivariate Cox regression method. Scores were added to the total score, which was then converted into linear predictor. The larger the positive number, the higher the value of risk to AS process it presents. The nomogram construction was carried out using the R package "rms". ROC curves were then constructed to evaluate the diagnostic capability of each potential gene in the development of AS plaques. The quantitative measure of the area under the curve (AUC) was calculated, with values greater than 0.7 considered significant.

2.8. Gene set enrichment analysis

Single-gene GSEA was conducted to investigate the possible roles of each candidate genes based on GO(c5.bp.v2023.2.HS.symbols.gmt, c5.cc.v2023.2.HS.symbols.gmt and c5.mf.v2023.2.HS.symbols.gmt) and KEGG term(c2.cp.kegg.v2023.2.HS.symbols.gmt) for each candidate genes. The version of GSEA software we utilized in our study was v4.3.1. Within the AS advanced plaque group, stratification into two subgroups was carried out on the basis of expression levels of each hub gene, using the median value of gene expression as the dividing criterion.

2.9. Immune infiltration analysis

CIBERSORT was employed to determine the relative proportion of immune cells within AS advanced plaque and control samples using tissue gene expression profiles. The analysis process was performed via "Cibersort" R package [18]. Subsequently, the proportion of distinct immune cell types and the comparison between the AS and control groups were visualized through bar plots and violin plots. Furthermore, the correlation between intersection genes and immune cell profiles were visualized.

2.10. Detection of hub genes and mediators associated subsets

Unsupervised consensus clustering method (K-means) was utilized to identify hub genes and mediators related subtypes in AS patients of GSE28829. The clustering methods "Pam" and "Ward's linkage" were implemented using the R package "ConsensuClusterPlus" and iterated 1000 times for reliable classification [19]. Then, "Cibersort" was utilized to examine the relationship between immune cells and genes. Finally, GSVA score between each subtypes was analysised with "Limma" package and "GSVA" package, with remarkable pathways displayed in heatmap.

2.11. Single-cell RNA sequence analysis

ScRNA datasets of AS plaque(GSE159677) was obtained from GEO database. The "Seurat" package was utilized for reading and analyzing of scRNA sequence [20,21]. To ensure data quality, the cells with the number of genes(nFeature RNA) < 200 or >4000, in addition to cells with >10 % mitochondrial mRNA were filtered out. Following data preprocessing, 2000 hypervariable genes were selected after performing Principal Components Analysis(PCA) dimensionality reduction and clustering. After analyzing JackStrawPlot and ElbowPlot, we chose the first 13 dimensions for subsequent analysis. Cell types were manually annotated based on 3 typical markers for each cell type with a mean expression count >2 in each cluster and expressed in more than 80 % of cells. DimPlot and

VlnPlot functions were utilized to visualize the cellular clusters and hub genes expression location after UMAP dimensionality reduction. “Monocle” R package was utilized for the pseudotime analysis of macrophage subtypes and the distribution of each hub genes.

2.12. CeRNA network construction

The Diana-microT 2023(interaction score>0.7), miRDB(score>50), miRWalk(score>0.9) and Targetscan were employed to obtain the prediction of potential miRNAs bindind to each candidate genes. Then, starBase was utilized to forecast the lncRNAs that target these miRNAs [22] The visualization of CeRNA network was then constructed via Bioinformatics platform.

2.13. Drug-protein interaction prediction

The drugs and molecules were predicted through CTD database. AutodockVina 1.2.5 was used to analyze the binding affinities and interaction modes of four identified candidate drugs [23]. Obtained from the Uniprot database was the 3D coordinates of the F13A protein with PDB ID 4kty and a resolution of 2.5 Å. The protein and molecular component files were transformed into PDBQT format, removing water molecules and introducing polar hydrogen atoms.

2.14. Statistical analysis

R version 4.3.0 was utilized to conduct WGCNA, GO enrichment, KEGG, and GSVA analyses. The ROC curve was using R package “pROC” and AUC calculation, along with the 95 % CI, was performed with SPSS Version 26.0.

3. Results

3.1. Identification of differentially expressed genes and enrichment analysis of atherosclerosis

In the combined AS plaque datasets, we identified 555 DEGs in total, with 453 genes showing up-regulation and 102 genes showing down-regulation in advanced plaques (see Fig. 1). Heatmap and volcano plot illustrate the DEGs in AS combined datasets(Fig. 2A and B). GO analysis showed that the biological processes(BP) of DEGs between AS and control were primarily involved in immune response include immune cells activation, migration, degraualation and chemotaxis process(Fig. 2C). GO analysis of cellular components(CC)

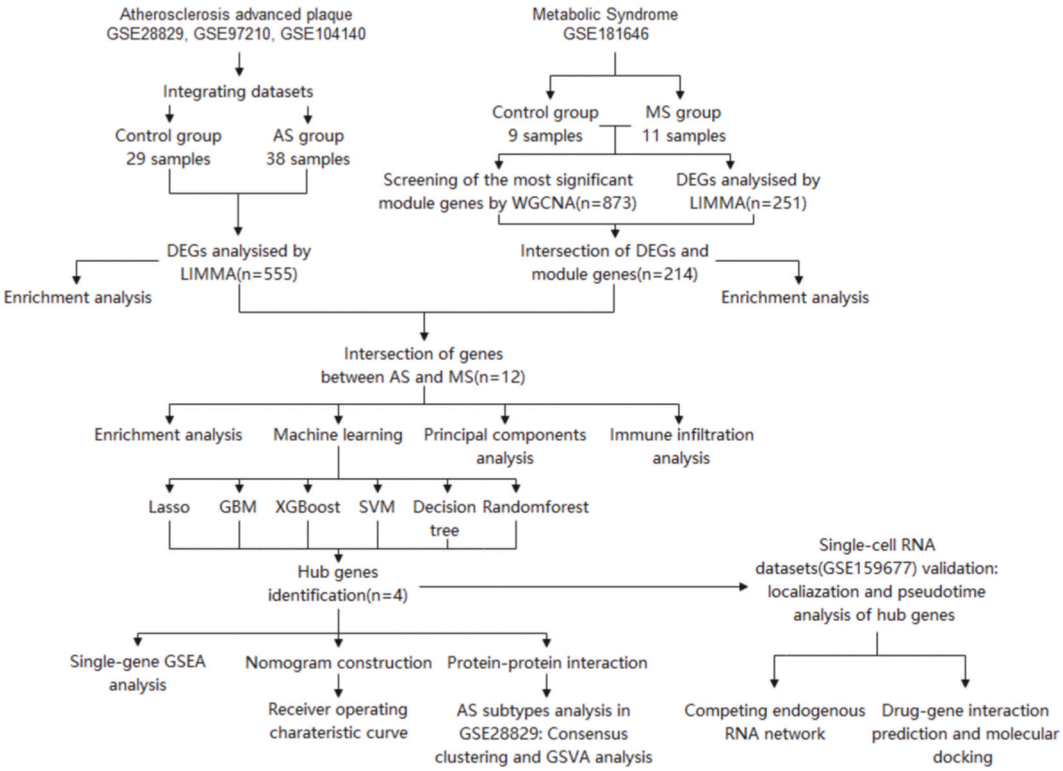

Fig. 1. Study flow chart.

exhibited that the DEGs were predominantly enriched in granule, membrane, lumen and chemokine activity(Fig. 2C). The GO analysis also emphasized the molecular functions(MF), showing enrichment in the function of chemokine, cytokine, Toll-like receptor binding, G-protein and intergrin(Fig. 2C). Regarding the KEGG enrichment analysis, the DEGs showed significant enrichment in pathways such

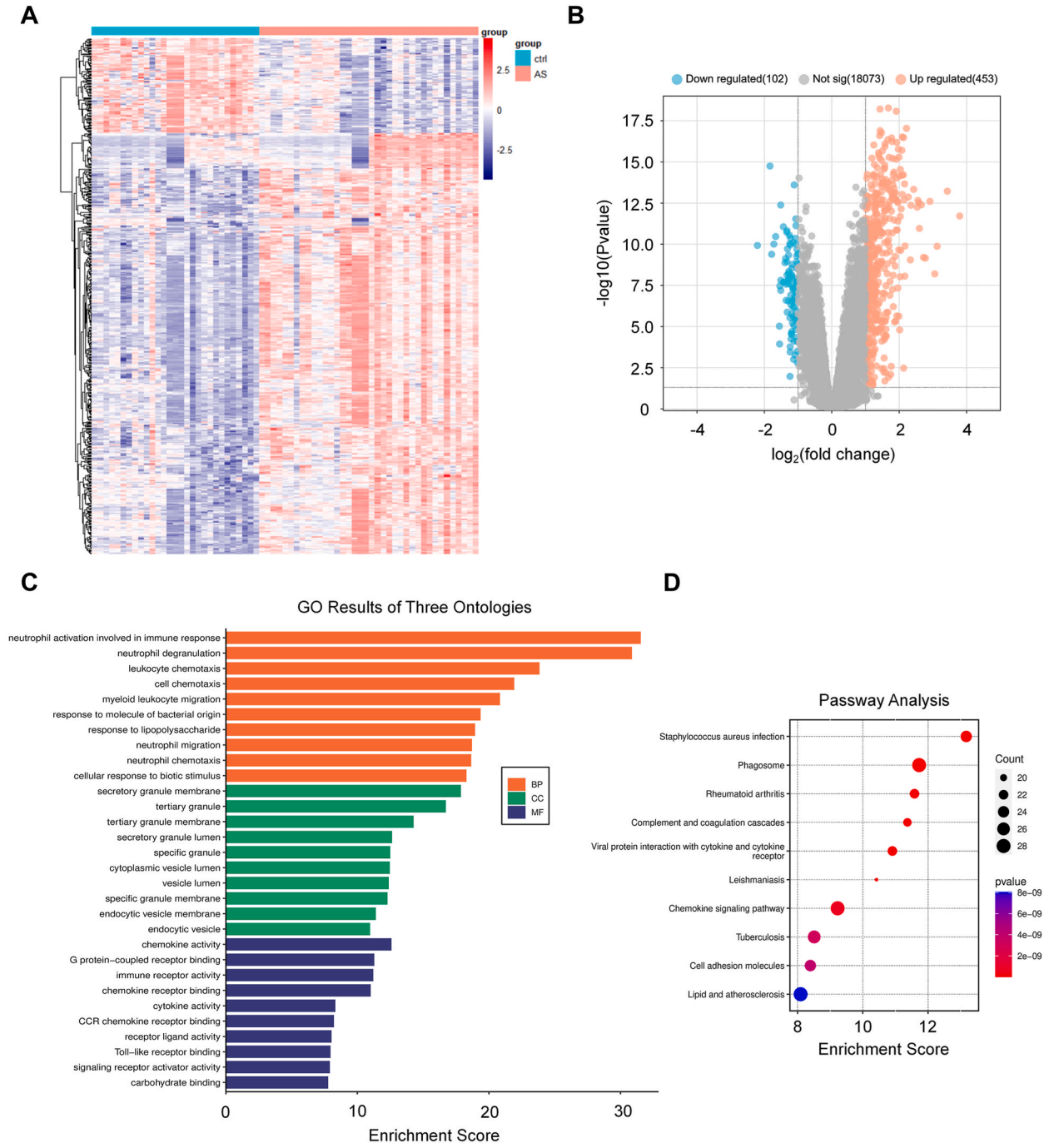

Fig. 2. DEGs identified form the integrated datasets of AS. (A) Heatmap for DEGs. DEGs are represented in each row, with each column corresponding to a sample of plaque from patients with AS or intima from the control group. The red represents up-regulated and blue represents down-regulated expression genes. (B) Volcano plot for DEGs. The red plots represents up-regulated and green plots represents down-regulated expression genes. (C) GO analysis of DEGs in AS. Enrichment score enriched in relative terms is represented on the x-axis, while different GO terms are represented on the y-axis. The circles' size indicates the number of genes, and the color indicates the p-value. (D) KEGG pathway analysis of DEGs in AS. On the x-axis, gene ratio enriched in various KEGG pathways is depicted, while the y-axis shows different KEGG pathways. (For interpretation of the references to color in this figure legend, the reader is referred to the Web version of this article.)

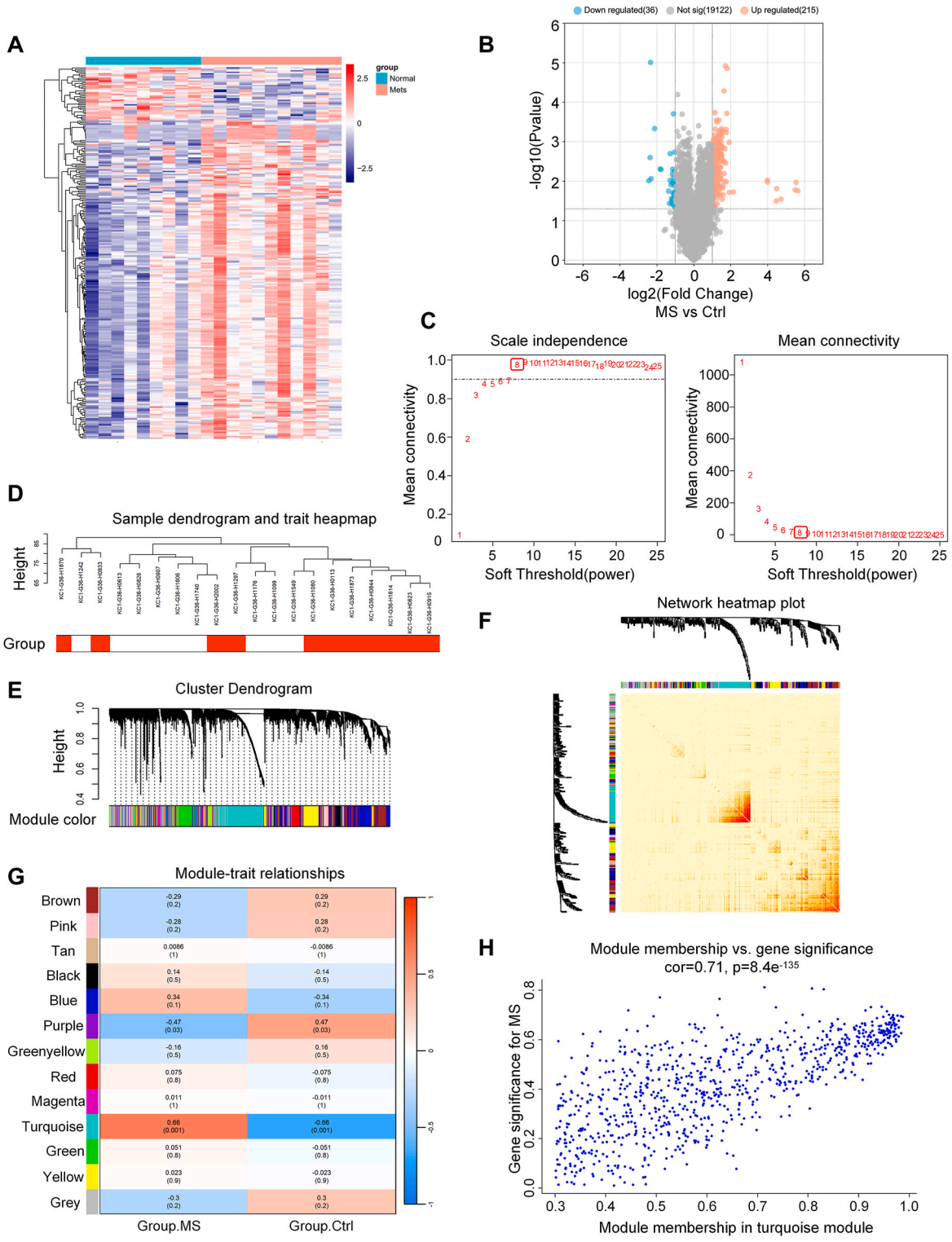

Fig. 3. DEGs were filtered and module genes were identified in MS. (A) Heatmap exhibits the DEGs identified in metabolic syndrome, while each row represents a DEG and each column represents a sample from either MS patients group or controls. The red area represents up-regulated and blue area represents down-regulated expression genes. (B) Volcano plot for DEGs. Each red plot represents up-regulated and each green plot represents down-regulated expression genes. (C) By analyzing both scale independence and average connectivity together, a soft threshold of $\beta = 8$ was chosen. (D) A dendrogram and heatmap displaying traits of both MS and control samples, with MS samples highlighted in red. (E) Different colors were vested as symbol of different gene co-expression modules identified in the clustering dendrogram. (F) Network heatmap plot of eigengene adjacency.

(G) Heatmap exhibits the relevance between each modules and MS. The turquoise module exhibits the most significant correlationship with MS. Numbers in each column represent correlation coefficient at to and p-value in the brackets. (H) Correlation plot exhibits the association between each membership and gene significance for genes found in turquoise module. Module membership is shown on the x-axis and gene significance for metabolic syndrome is shown on the y-axis. (For interpretation of the references to color in this figure legend, the reader is referred to the Web version of this article.)

as "*Staphylococcus aureus* infection", "Phagosome", "Rheumatoid arthritis", "Complement and coagulation cascades", "Viral protein interaction with cytokine and cytokine receptor" and et al.(Fig. 2D). Detailed enrichment genes, pathways, biological process, cellular components and molecular functions genes are listed in Supplemental Table 1. Fig. 3A and B displays the DEGs in PBMCs of MS patients and healthy individuals using a heatmap and volcano plot. Among these, there was an increase in expression of 215 genes and a decrease in expression of 36 genes.

3.2. Key module identification in metabolic syndrome

WGCNA was processed to discover the significant and related gene module expressed in MS. We chose $\beta = 8$ (scale-free $R2 = 0.9$) as threshold power, on the basis of scale independence and mean connectivity(Fig. 3C). The dendrogram and heatmap of traits for the MS patients group and control are displayed in Fig. 3D. Fig. 3E–G presents that there are 13 gene co-expression modules shown in the cluster dendrogram, network heatmap plot, and module-trait relationship heatmap. The module distinguished with turquoise color, consisting of 873 genes, showed the most proximal correlation with MS (correlation coefficient = 0.66, $p = 0.001$). Fig. 3H illustrated each membership and their relationship with gene significance in the turquoise module, showing a significant positive correlation(cor = 0.71). Consequently, the turquoise module was chosen for further examination.

3.3. Functional enrichment analysis of metabolic syndrome

GO and KEGG enrichment analysis were then employed to asses the pathologenesis characterist of MS datasets. 214 common genes were found by intersecting DEGs and significant module genes in WGCNA (Fig. 4A). Analysis of KEGG pathway showed that these common genes were significantly overrepresented in terms such as "Platelet activation", "ECM-receptor interaction", "Focal adhesion", "Hypertrophic cardiomyopathy", "Dilated cardiomyopathy", "Gap junction", "Regulation of actin cytoskeleton", "Hematopoietic cell lineage", "cGMP-PKG signaling pathway" and "Arrhythmogenic right ventricular cardiomyopathy"(Fig. 4B). Analysis of GO showed that common genes were primarily concentrated in processes related to "blood clotting", "blood flow regulation", "platelet activity", and "cell attachment"(Fig. 4C). Function analysis from GO showed that common genes were predominantly associated with "actin", "extracellular" matrix", "sulfur compound", and "chemokine binding functions"(Fig. 4D). CC analysis from GO revealed that shared genes were predominantly concentrated in "platelet granule", "vesicle lumen" and "cytoskeleton components"(Fig. 4E). Detailed enrichment data are demonstrated in Supplemental Table 2.

3.4. Identification of intersection gene and functional enrichment analysis

To further excavate the relationship between significant genes in MS and AS, we identified 12 intersection genes between DEGs from AS and intersection module genes from MS(Fig. 5A). PCA analysis of the integrated gene expression matrix indicated distinct clustering and differentiation between AS and control groups, with samples clearly distributed on opposite sides based on these intersection genes(Fig. 5B). To further delve the function and mechanism of intersection genes, GO and KEGG analysis were then conducted. KEGG pathways showed that there was enrichment of intersection genes in categories such as "Coronavirus disease", "Complement and coagulation cascades", "Relaxin signaling pathway", "Focal adhesion", "PI3K-Akt signaling pathway" and et al. (Fig. 5C). BP of GO revealed that intersection genes were primarily enriched in "coagulation", "hemostasis", "BMP signaling" and "cellular response"(Fig. 5D). MF of GO demonstrated that intersection genes were mainly enriched in "serine-type peptidase regulation", "glutamic acid ligase activity", "cell signal binding" and "extracellular matrix structural regulation"(Fig. 5E). CC of GO showed that common genes were mainly enriched in "vesicle", "granule lumen" and "collagen-containing extracellular matrix"(Fig. 5F). Detailed enrichment data are shown in Supplemental Table 3.

3.5. Identification of candidate hub genes with machine learning

Various machine learning algorithms, including LASSO regression, GBM, RF, XGboost, SVM-RFE and decision tree algorithms, were then utilized to pinpoint potential hub genes for creating a nomogram and assessing diagnostic value. LASSO regression identified 7 candidate genes(Fig. 6A and B), while GBM identified 10 feature genes with importance score >0(Fig. 6C). RF algorithms ranked all of the genes and we chose top 10 as feature genes(Fig. 6D and E). Based on the selection of optimization parameters, SVM-RFE identified 11 feature genes(Fig. 6G and H), which the same with XGboost(Fig. 6F). 8 feature genes were ranked through decision tree algorithms based on the importance score(Fig. 6I). Overall, 4 genes include F13A1, MMRN1, SLCO2A1 and ZNF521 were identified as common among all of the candidate genes identified by machine learning algorithms(Fig. 6J). F13A1, MMRN1, SLCO2A1 and ZNF521 could potentially interact directly with each other or through mediators(Fig. 6K). The relative gene expression level of each hub genes in across different cohorts was exhibited in Figure S3.

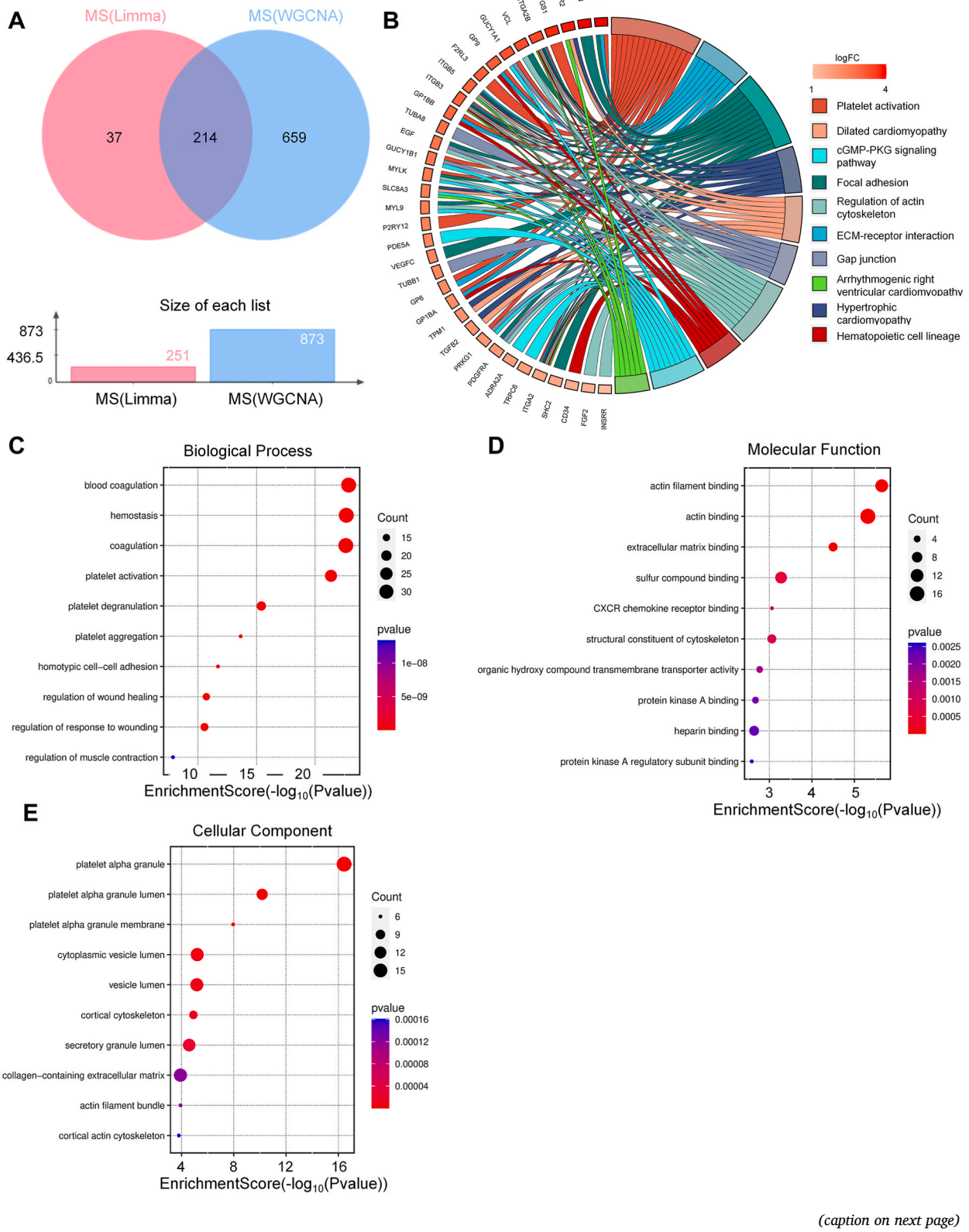

(caption on next page)

Fig. 4. Analysis of overlap genes between DEGs and WGCNA analysis in MS datasets. (A) Venn diagram indicates the overlap of 214 genes between DEGs and module genes. (B) Conducting KEGG pathway analysis on overlap genes. Various hues symbolize the top 10 important pathways and their associated enriched genes. (C–E) Analysis of GO. Enrichment score in relative terms is represented on the x-axis, while different GO terms of BP, CC, and MF are represented on the y-axis. The circles's size indicates the number of genes, and the color indicates the p-value. (For interpretation of the references to color in this figure legend, the reader is referred to the Web version of this article.)

3.6. Diagnostic value assessment of candidate hub genes

A nomogram was created with 4 potential hub genes, and ROC curves were then generated to assess the sensitivity and specificity of each gene, along with the nomogram point(Fig. 7A). All gene expression counts were transferred into log as relative levels, and then converted into scores. The sensitivity and specificity of F13A1(AUC 0.965, CI 0.927–1.000), SLCO2A1(AUC 0.877, CI 0.795–0.960), MMRN1(AUC 0.818, CI 0.716–0.919), ZNF521(AUC 0.920, CI 0.849–0.991), along with the nomogram point(AUC 0.979, CI 0.953–1.000) were presented in Fig. 7B–F. The results demonstrated that the four candidate genes and the constructed nomogram collectively exhibited a high diagnostic value for AS of MS patients.

3.7. Gene set enrichment analysis for candidate hub genes

The pathways and functions associated with the 4 candidate genes were excavated through a Single-gene GSEA analysis. Genes that showed differencially expression between high and low level of each hub genes were highly enriched in pathways of "chemokine signaling", "cytokine interaction", "lyososome", and "activation of immune response process"(Fig. 8A–H and Supplemental Fig. 1A-H). These findings provide strong evidence that the 4 hub genes are closely associated with immune and inflammation responses in the context of AS. Detailed enrichment data are illustrated in Supplemental Table 4.

3.8. Immune cell infiltration analysis

After observing that the genes common to both AS and MS were primarily linked to immune and inflammation process, we then proceeded to conduct an analysis of immune cell infiltration to pinpoint the specific cell types of immune infiltration in the plaque. Fig. 9A displayed the distribution of 22 different immune cell types in each samples within AS advanced plaque and control groups (Fig. 9A). A comparison revealed lower levels of immune cells, including plasma cells, resting $CD4^+$ T cells, monocytes, activated dendritic cells, and resting mast cells, and higher levels of cells, such as B memory cells, activated memory $CD4^+$ T cells, M0 macrophages, and M2 macrophages, in AS advanced plaque samples(Fig. 9B). Furthermore, the connection between 4 hub genes and different type of infiltrarion immune cells were exhibited. Although 4 hub genes showed different correlation with immune cells, all of them seem highly correlated with macrophages(Fig. 9C).

3.9. Association between infiltrating immune cells and AS subtypes

To further investigate the correlation between immune infiltration and hub genes, we identified the hub genes and mediators related subtypes in AS with the using of consensus clustering analysis(Fig. 10A–B). Two clusters were identified in AS patients after comparing the level of hub genes and mediators related with immune infiltration. Cluster2 showed higher infiltration of M2 macrophages(Fig. 10C–E). GSVA analysis indicated that cluster1 showed higher enrichment in "primary immunodeficiency", "porphyrin and chlorophyll metabolism", "alanine aspartate and glutamate metabolism" and "ribosome". Cluster2 showed higher enrichment in "focal adhesion", "ECM receptor interaction", "gap junction", "inositol phosphate metabolism", "NOTCH pathway" and so on, which mainly correlated with immune infiltration and migration and indicated its immune correlation role(Fig. 10F).

3.10. ScRNA sequencing analysis

We proceeded with single-cell RNA sequencing analysis to validate the high expression of each hub gene in AS plaque and determine their specific locations. After dimension reduction and clustering, the visualization of UMAP revealed that F13A1 exhibited high expression primarily in monocytes and macrophages within the AS plaque, while MMRN1, SLCO2A1 and ZNF521 were found to be highly expressed in endothelial cells(Fig. 11A–E, Figure S2A). Macrophages were then divided into 4 subtypes which identified as C1q + macrophages(with high expression of C1QA, C1QB, C1QC and F13A1), SPP1+ macrophages(with high expression of SPP1, CSTB and CD36), S100A + macrophages(with high expression of S100A8, S100A9 and FCN1) and S100B + macrophages(with high expression of S100B, DNASE1L3 and IDO1) (Fig. 11F, Figure S2B). Pseudotime analysis identified the differentiation locus of 4 macrophage subtypes and F13A1 showed the centralization in the differentiation of C1q + macrophages(Fig. 11G–H), which indicates the regulation mechanism of the macrophages differentiation in AS plaque processing. No significant differentially expression was found in differentiation locus of macrophages for ZNF521, SLCO2A1 and MMRN1.

3.11. Construction of ceRNA network

We constructed ceRNA network on the basis of competitive endogenous RNA theory, aiming to uncover the lncRNAs that act as

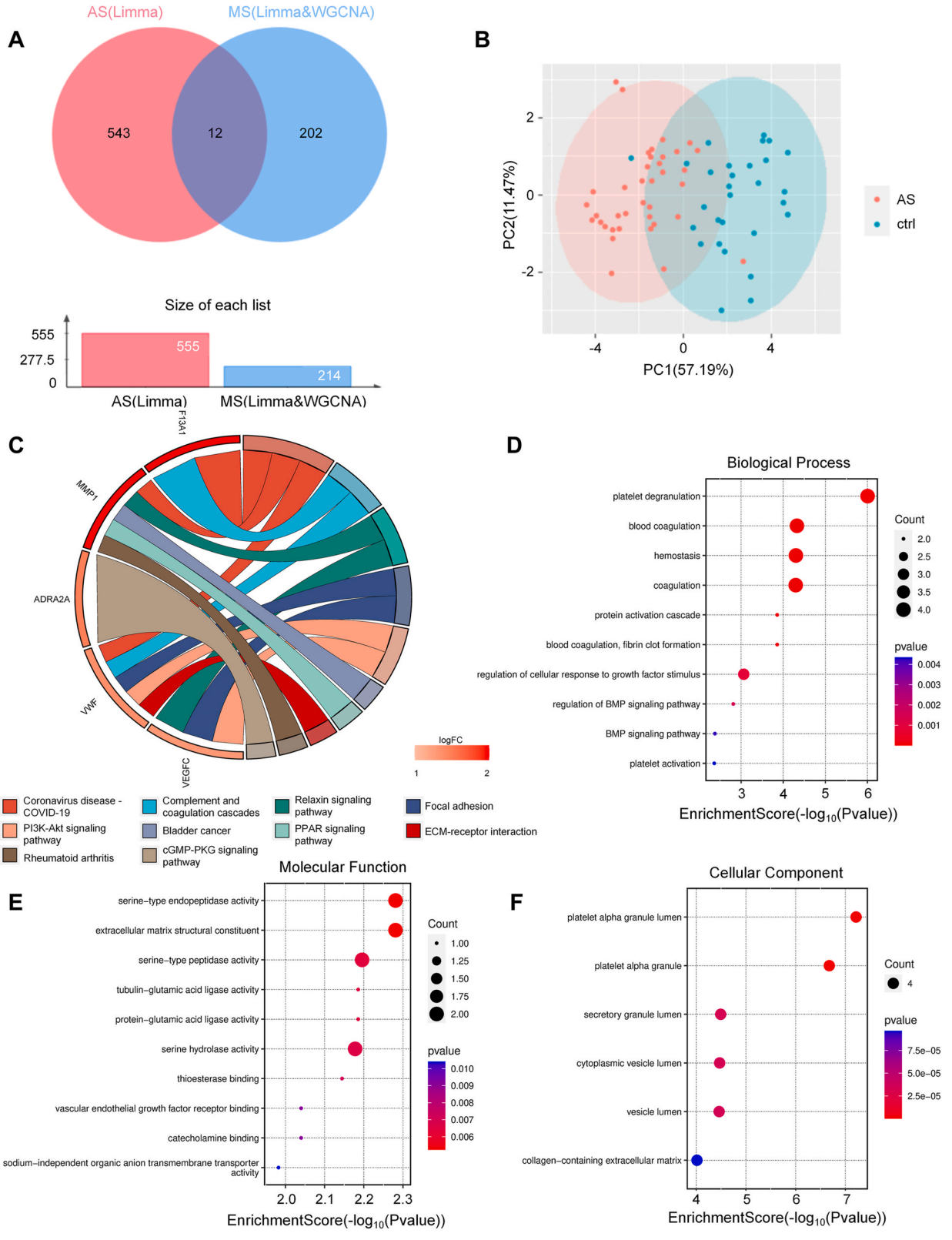

(caption on next page)

Fig. 5. Analysis of intersection genes form AS with MS. (A) A Venn diagram exhibits that 12 common genes were found among differentially expressed genes in AS and significant genes in MS. (B) The sample distribution patterns were analyzed using PCA results in combined AS datasets. (C) KEGG pathway analysis of 12 intersection genes. Various hues symbolize the top 10 important pathways and their associated enriched genes. (D–F) Analysis of the intersection genes using GO. Enrichment score in relative terms is represented on the x-axis, while different GO terms of BP, CC, and MF are represented on the y-axis. The size of the circles indicates the number of genes, and the color indicates the p-value. (For interpretation of the references to color in this figure legend, the reader is referred to the Web version of this article.)

miRNA sponges in AS plaque progress with MS. This network amalgamates F13A1 along with predicted miRNAs and lncRNAs. Totally 6 miRNA nodes and 164 lncRNA nodes were contained in the ceRNA network(Fig. 12A), which exhibits the potential regulation mechanisms of F13A1.

3.12. Prediction of candidate drugs and the binding modes for F13A1

Molecular docking analysis was conducted to determine the candidate drugs' attraction to F13A1. Four candidate drugs(Carfentanil, with the binding energy of −7.906 kca/mol; Iodoacetamide, with −3.556 kca/mol binding energy; Senecionine, with −7.836 kca/mol binding energy and Valproic Acid, with −4.795 kca/mol binding energy) were identified and each of them could bind to F13A1 through hydrogen binds and strong electrostatic interactions(Fig. 12B–E). The low binding energy indicates the highly stable binding for each drugs to F13A1.

4. Discussion

AS stands as a major global public health concern, driving the leading cause of death. Notably, metabolic syndrome emerges as an independent rick factor amplifying AS progression. Although previous research has delved into some biomarkers that tied to the mechanism of chronic inflammation, oxidative stress, dyslipidemia, endothelial dysfunction and marrow dysregulation [24–28], the potential genomic diagnostic and therapy biomarkers within MS patients that may underlie the formation and advancement of AS plaque remain uncovered yet. Furthermore, the potential of integrating machine learning and nomogram analysis for diagnosing AS plaque progression in MS patients population was untapped. After comprehensive exploration encompassing bioinformatics and machine learning analysis, nomogram and ROC curve were established and the diagnostic value for AS plaque progress in MS patients was evaluated. Four immune-correlated hub genes were identified include F13A1, MMRN1, SLCO2A1 and ZNF521 and evaluation of their diagnostic potential was conducted both collectively and individually.

Samples in MS datasets comprised peripheral blood mononuclear cells, which could be easily obtained from blood, ensuring the convenience and acceptance of patients. It facilitates the assessment of gene expression for the 4 hub genes, enabling the utilization of a diagnostic method based on peripheral blood samples to gauge the likelihood of AS plaque progression [29]. Although each of the 4 hub genes exhibits potential as independent diagnostic marker, we further constructed a comprehensive diagnosis model by combining all 4 hub genes. Each gene's expression level was quantified and converted into a corresponding score, which collectively contributed to the linear predictor. Elevated risk of AS plaque formation and advancement would be effectively predicted with the linear predictor and early intervention strategies could be implemented.

In atherosclerosis, the damage of the endothelial lining and the adhesion of platelet to endothelium were the early stage of atherosclerosis plaque formation. Enrichment of hub genes were mainly concentrated in platelet activation, ECM-receptor interaction and focal adhesion, which are the early stage of endothelium dysfunction and these process promote aggregation of platelet and inflammation cells. Multimerin 1 (MMRN1) belongs to the EMILIN/multimerin family and is primarily expressed in endothelial cells, platelets, megakaryocytes, and the extracellular matrix. In vivo, MMRN1 has a crucial function in platelet attachment and controlling coagulation factor V [30–33]. In situations of intense shear stress, MMRN1 has been observed to interact with von Willebrand factor (VWF), enhancing platelet adhesion to the endothelium [32], while high shear stress is also linked to dysregulation of endothelial function and early formation of AS plaque [34,35]. Our study verified the high expression in endothelium of MMRN1, which indicated that MMRN1 may promote the adhesion of platelet to endothelium and formation of early AS plaque. Besides, GSEA analysis also indicated that MMRN1 promote the activation of immune response.

Both innate and adapted immune systems play integral roles in the process of AS plaque formation [36]. Elevated cholesterol levels stimulate monocyte proliferation, and the chemokine CCL2 facilitates monocyte recruitment to the plaque [37–39]. Monocyte-derived macrophages contribute to the absorbing of lipoproteins and creating of foam cells, ultimately contributing to the development of early atherosclerotic plaque [40]. As we observed in our study, M0 and M2 macrophages are increased in AS plaque without M1 macrophages, of which M1 macrophages are known as pro-inflammatory cells [41], which needs further investigation to validate. F13A1 was found to be a co-expression gene with M2 macrophages infiltration and may play critical role in immune response of AS progress [42]. Within the adaptive immune system, T helper-1 (Th1) T cells, as well as Th17 and Th2 T cells involves in inflammatory adaptive immune response in AS plaque formation [43]. The research we conducted revealed a connection between SLCO2A1 and $CD4^+$ and $CD8^+$ T cells, which indicates that it may affect the adaptive immune system. As SLCO2A1 regulates the distribution of PGs, PG signaling and inflammatory response in vivo and vitro [44,45], it mainly inhibits the endothelial cell migration, angiogenesis and wound healing, which induces the hypertrophic osteoarthropathy, chronic enteropathy and hypertension [46–48]. There is no evidence illustrating its role in the development of AS. The regulatory functions of SLCO2A1 in angiogenesis, endothelial migration, correlation with T cells and its possible involvement in early AS plaque formation are significant considerations.

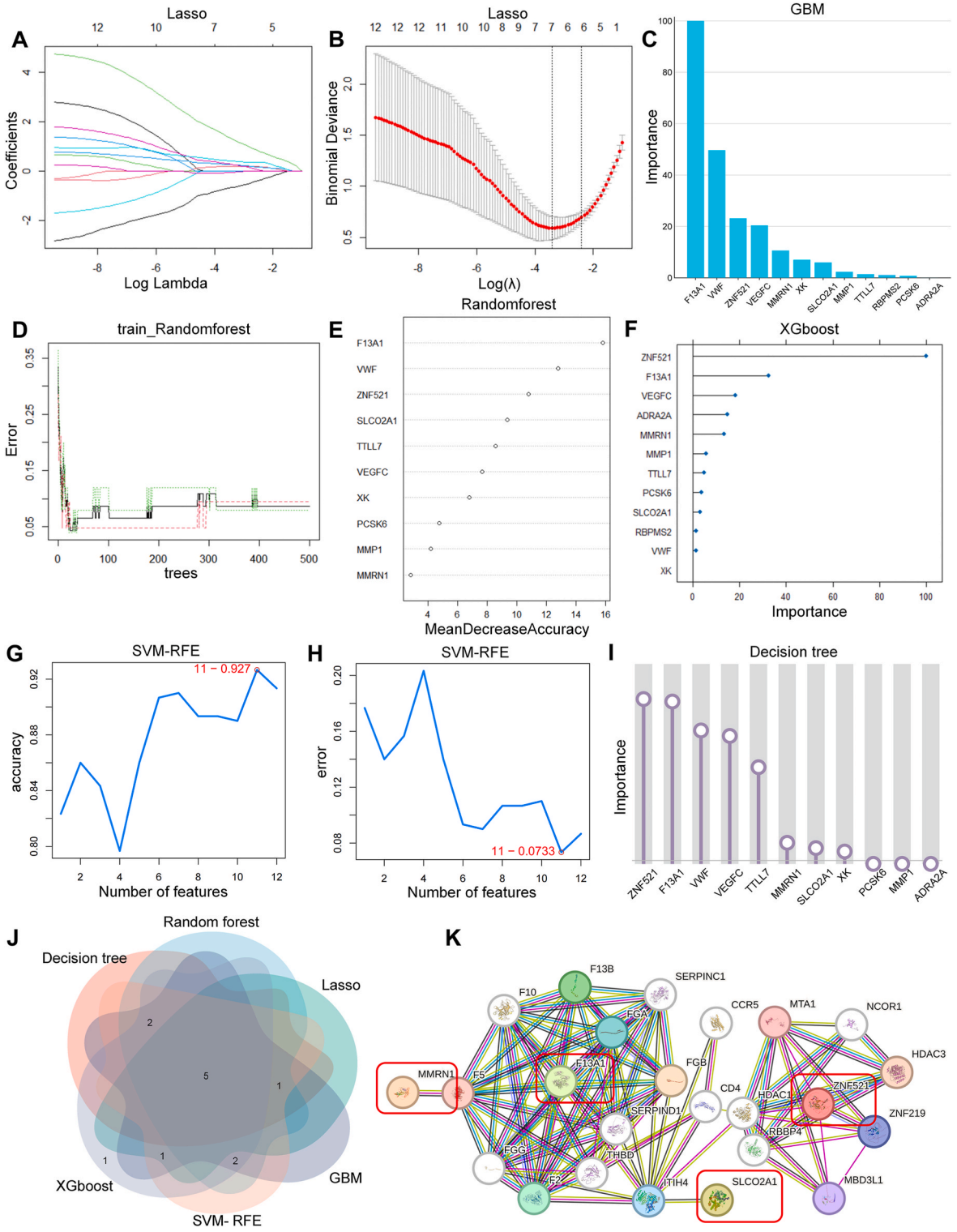

Fig. 6. Machine learning in identificating candidate genes for AS with MS. (A, B) LASSO model. The 7 genes that align with the lowest point of the curve were the most appropriate for diagnosing AS with MS. (C) Barplot indicates the rank of importance among 12 genes with the utilize of Gradient Boosting Machine(GBM) algorithm. 10 genes with importance score >0 was selected as feature genes. (D, E) The error tree and gene ranking based on importance scores were displayed by the random forest algorithm. (F) XGBoost algorithm was used to screen candidate genes and rank them according to their importance scores. 10 genes with importance score >0 was selected as feature genes. (G, H) Line charts show that 11 genes with the highest point of accuracy curve and lowest point of error curve were selected as feature genes with the utilize of SVM algorithm. (I)

Candidate genes screening in decision tree model. 8 genes with importance score >0 was selected as feature genes. (J) Venn diagram indicates that 4 candidate hub genes for AS with MS diagnosis are identified from intersection with LASSO model, GBM algorithm, random forest algorithm, XGBoost algorithm, SVM algorithm and decision tree model. (F) PPI network shows the interaction of 4 hub genes and the mediator molecules. Red frames indicate the 4 hub genes. (For interpretation of the references to color in this figure legend, the reader is referred to the Web version of this article.)

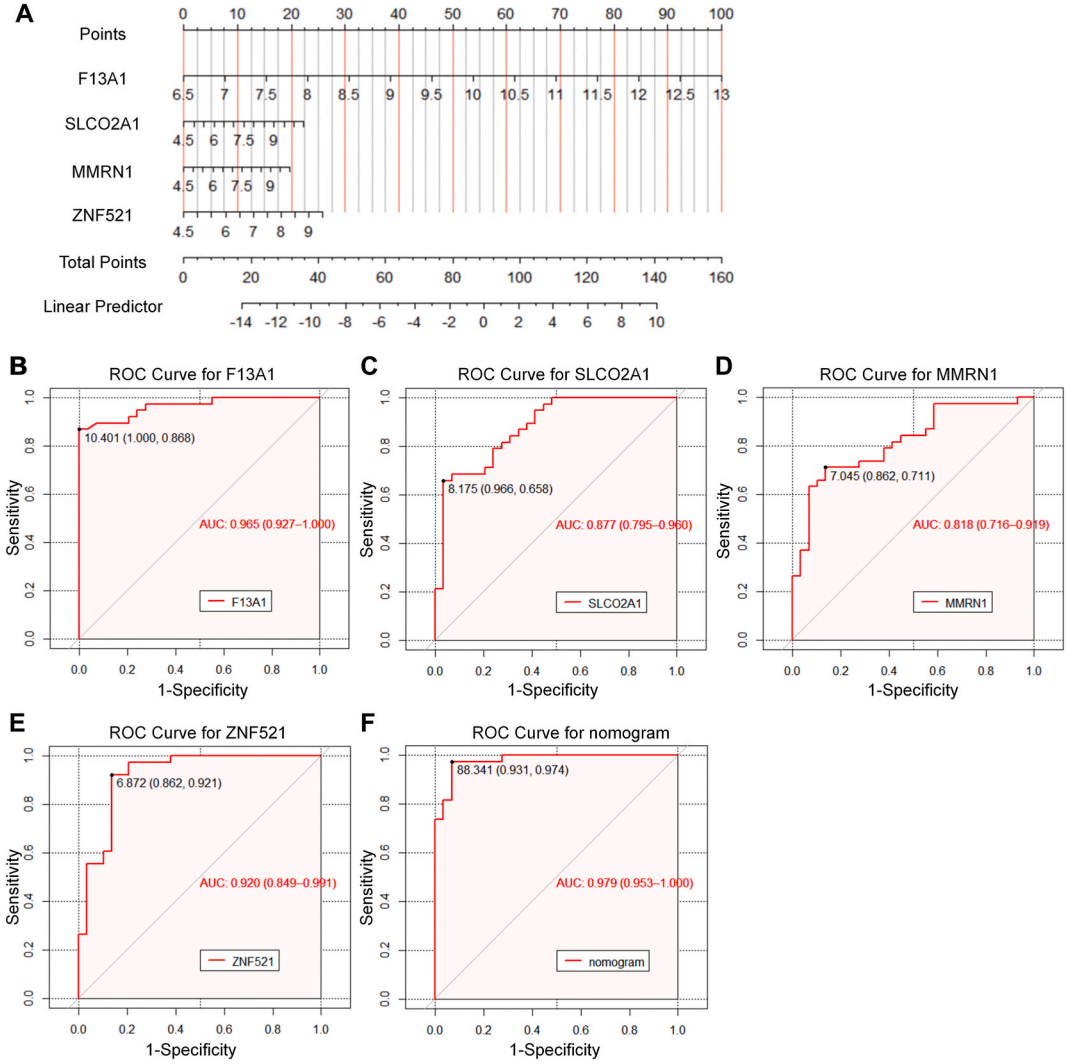

Fig. 7. Nomogram construction and the evaluation value of diagnose. (A) Visualized nomogram was created to predict AS in individuals with MS. (B–F) The ROC curve of F13A1, MMRN1, SLCO2A1, and ZNF521, along with the total nomogram score, demonstrated the considerable diagnostic accuracy of atherosclerosis in individuals with metabolic syndrome.

B lymphocytes have a dual function in the immune system, releasing both anti-inflammatory and pro-inflammatory signaling molecules, along with antibodies [49]. B1 cells contribute to the innate immune system, while B2 cells rely on T follicular helper cell activation. IRA-B cells are implicated as pro-atherogenic and could drive myeloid cell activation and pro-atherogenic TH1 immunity, while conversely, B-regulatory cells secrete anti-inflammatory cytokines and activate T-regulatory cells [50–52]. ZNF521, a zinc finger protein, acts as a crucial co-transcription factor in the regulation of hematopoietic, neural, and mesenchymal stem cells, as well as holds significant importance in tumor formation and development [53]. ZNF521 was found to be correlated with cell differentiation of B cells in our study, which indicates that it may participate in innate immune regulation. Notably, ZNF521 could up-regulate the c-myc, c-jun and Ccnd3, which encodes cyclin D3 and subsequently induces the growth of pre-B cells and immature B cells [54]. As we conjectured, ZNF521 stimulated the generation of immature B cells, which further differentiate into follicular dendritic cells. With the help of T helper cell, it transfer to follicular B cells, which secret IgG, activate inflammatory T cells and further induces the inflammation and immune infiltration in AS plaque [55]. It may be a targets for inhibits the early immune activation and potential

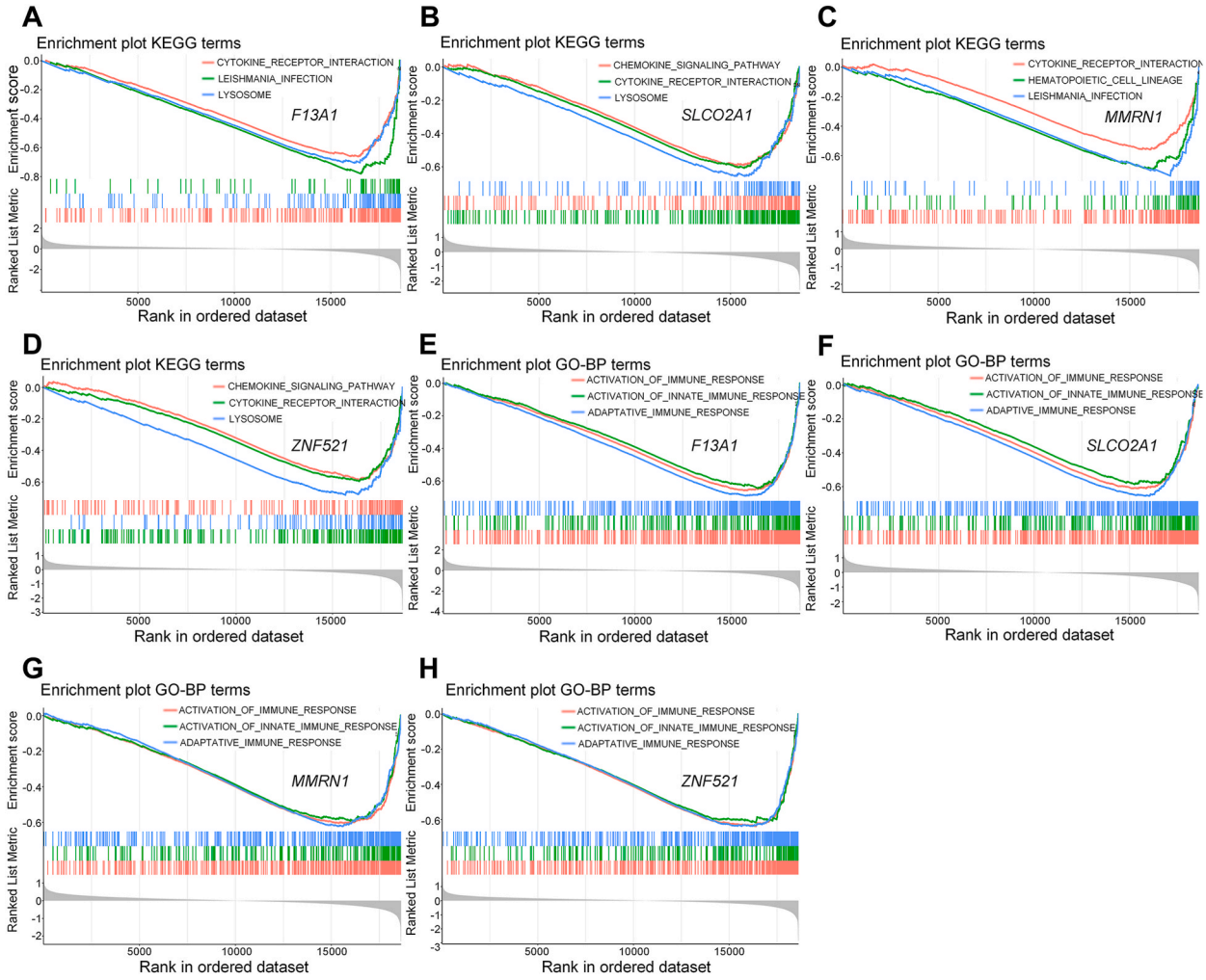

Fig. 8. Single gene GSEA for 4 candidate genes. (A–D) Top 3 co-enriched KEGG terms of pathway enrichment for each candidate gene via single gene GSEA. (E–H) Top 3 co-enriched GO-BP terms of biological process for each candidate gene via single gene GSEA.

therapeutic and prevention targets of AS in MS patients. Our investigation revealed that the AS patients' plaque could be categorized into two subtypes using hub genes and mediators expression profiles, which exhibited varying levels of M2 macrophage infiltration. These finds indicate that 4 hub genes and their interaction-relative genes may regulate the function and polarization of macrophages synergistically.

Factor XIII-A transglutaminase, encoded by F13A1, functions as a pivotal enzyme within coagulation cascade and exerts the ability to cross-link fibrin fibers and platelet with endothelium, thereby ensuring the stablization of neo-formed coagulation clot [56]. Beyond its role in coagulation, Factor XIII-A exhibits significance in wound healing, alleviating skin sclerosis, arthralgia, and enhancing microcirculation function in systemic sclerosis [57–59]. It greatly reduces the production of thrombospondin-1 (TSP-1), a factor that inhibits blood vessel formation and increases the protein Bax, which promotes cell death, while decreasing the protein Bcl-2 [60]. F13A1 was also found as a marker in M2 macrophages in the activation of inflammation and immunity [61]. The FXIII-A activation could increase the adhesion of monocyte to endothelium, mediate the phagocytosis of monocytes, promote the remodeling of small arteries and stimulate vascular smooth muscle cell migratio [62–65]. Given the elevated presence of M2 macrophages in atherosclerosis plaques and high expression in macrophages via scRNA analysis observed in our study, F13A1 holds potential as a biomarker in the infiltration of alternative macrophages and the formation of advanced plaque. The pro-phagocytosis and pro-adhesion function of F13A1 healing function of Factor XIII-A may another reason for the differential expression of FXIII-A in monocytes may induces the aggregation of macrophages and formation of foam cells, which was the main components of AS plaque. But the mechanism needs further study to investigate.

In single-cell RNA sequence analysis, no significant high expression was found in macrophages for these 3 hub gene. However, the high expression of MMRN1, SLCO2A1, and ZNF521 in endothelial cells and the pathways showed in enrichment analysis of cluster2 subtypes also suggest that these genes may participate in immune adhesion and migration of endothelium in early stage of AS plaque

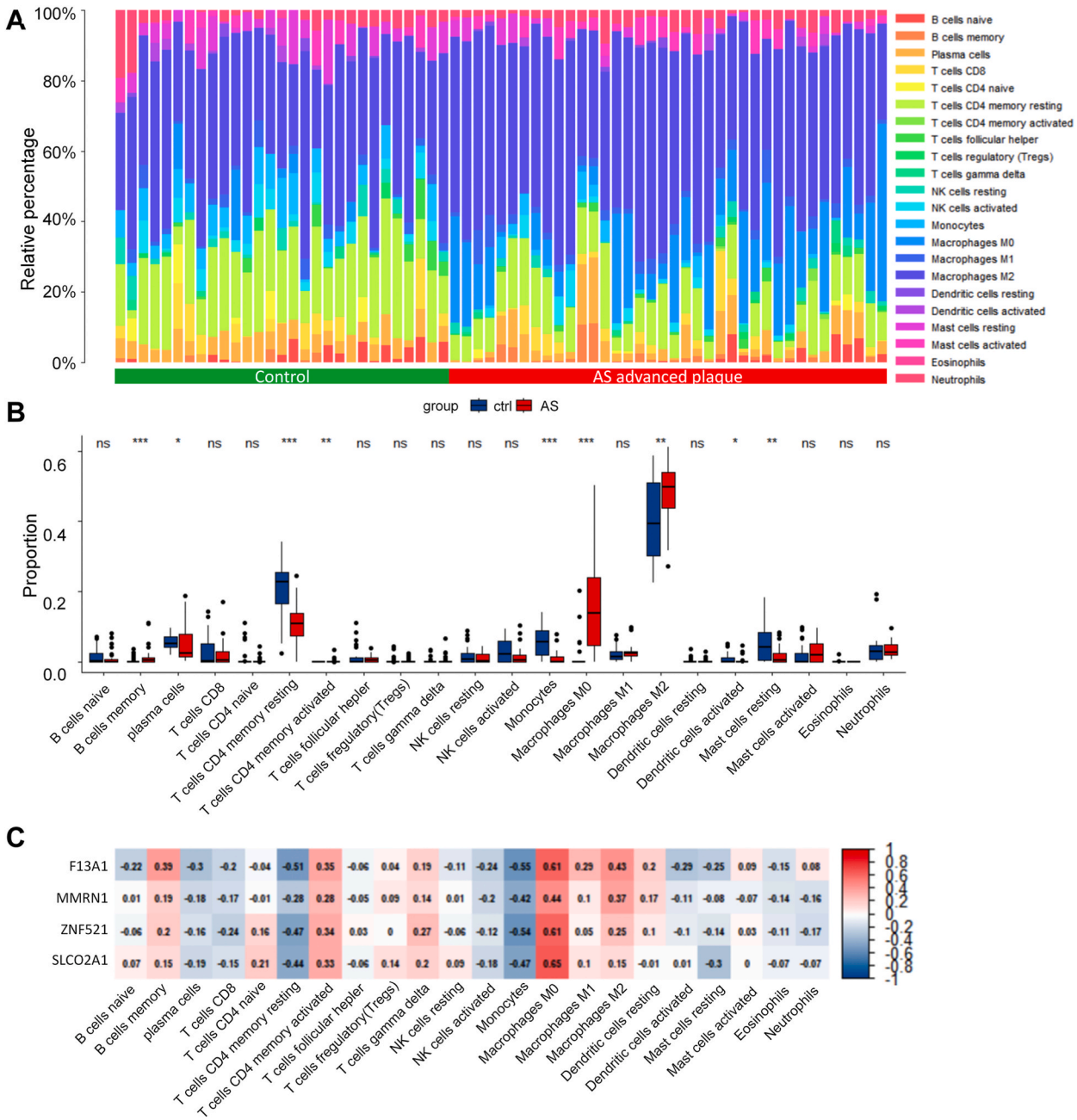

Fig. 9. Comparison of immune cell infiltration in individuals with AS and those in the control group. (A) Barplot indicates the distribution of 22 types of immune cells in various AS and control specimens. (B) Vioplot illustrates the contrast in the distribution of 22 different types of immune cells between the AS and control groups. (*, $p < 0.05$, **, $p < 0.01$, ***, $p < 0.001$.) (C) Heatmap shows the correlation between 4 hub genes and 22 kinds of immune cells.

formation. These genes may stimulate immune infiltration and inflammatory adhesion, as they all exhibit some level of activity as stimulators of immune adhesion and inflammation activation. Nevertheless, the specific functions and mechanisms of each gene in endothelial cells require further study for validation.

We revealed that F13A1 mainly expressed in monocytes and macrophages within AS plaque. Pseudotime analysis in single-cell sequence exhibited the potential differentiation direction and polarization process of macrophages in the processing of AS. Four type of macrophages were excavated and we defined them as C1q + macrophages, SPP1+ macrophages, S100A + macrophages and S100B + macrophages. The enriched expression and high correlation of F13A1 within C1q + macrophages identified its regulation function in cell subtypes differentiation locus. As C1q was found to modulate the differentiation of monocytes to M2 macrophages

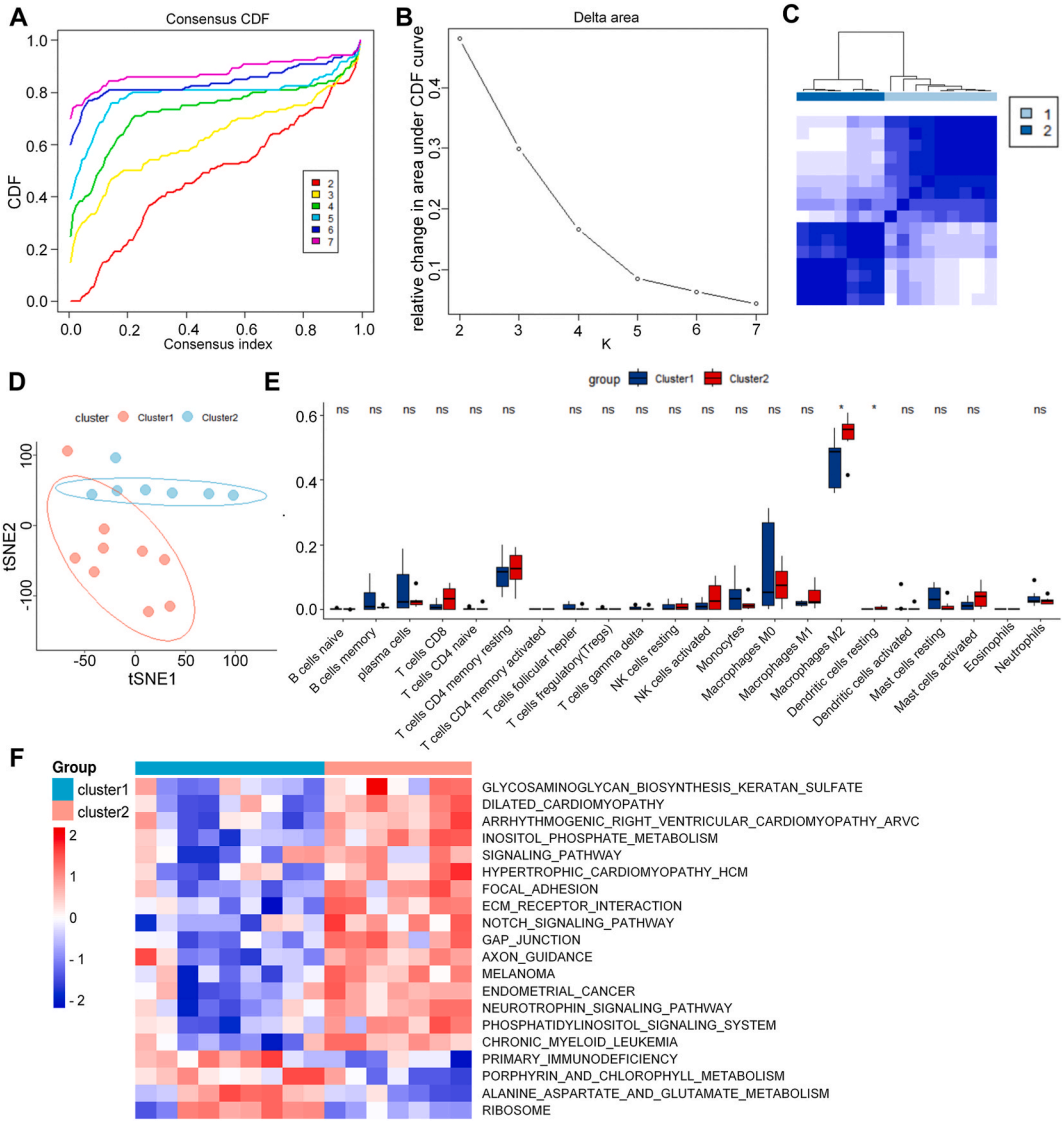

Fig. 10. Consensus clustering analysis based on GSE28829. (A–B) Consensus cumulative distribution function(CDF) for k values ranging from 2 to 7 and changes in the relative area under the CDF curve. (C) Consensus matrix heatmap exibits AS cohorts when k = 2. (D) The dot map displays the distribution features of the samples using tSNE analysis. (E) Violoplot displays the contrast in the distribution of 22 different immune cell types among 2 subcategories. (F) GSVA analysis revealed distinct pathway distributions between the 2 subtypes.

[66], our observation aligns with F13A1 being a marker for M2 macrophages, indicating its involvement in the activation of inflammation and immunity.

The miRNAs and lncRNAs integrated into ceRNA network were computationally predicted to unravel the potential competitive regulation components. Considering miRNAs' inhibitory role in mRNA targeting, the sponge-like function of these lncRNAs may act as promoters to F13A1 [67–69]. These components may be potential intervention and therapeutic targets in MS patients with high risk of AS plaque advancement. However, rigorous investigation is essential to validate the function and mechanism of these miRNAs and lncRNAs. Four medications were discovered that interacted with F13A1, offering a possible approach to influencing the development of macrophages and the advancement of AS plaque. Carfentanil and Senecionine could increase the expression and activity of F13A pretein, while Iodoacetamide and Valproic Acid performed the opposed function. Carfentanil is a synthetic fentanyl analogue and no evidence shows its function association with AS, while Senecionine was found that could induce the mitochondria-mediated apoptosis in mice [70]. In previous study, Iodoacetamide was found playing antioxidant role in endothelial cells through increasing HO-1, which F13A1 could be another potential target for its antioxidant process [71]. Recent study also found that Valproic Acid could decrease SMC proliferation and could be potential treatment of atherosclerosis [72], which F13A1 may be another targets in atherosclerosis prevention and intervention.

In summary, we have identified 4 immune-associated hub genes (F13A1, MMRN1, SLCO2A1 and ZNF521) that serve as novel and

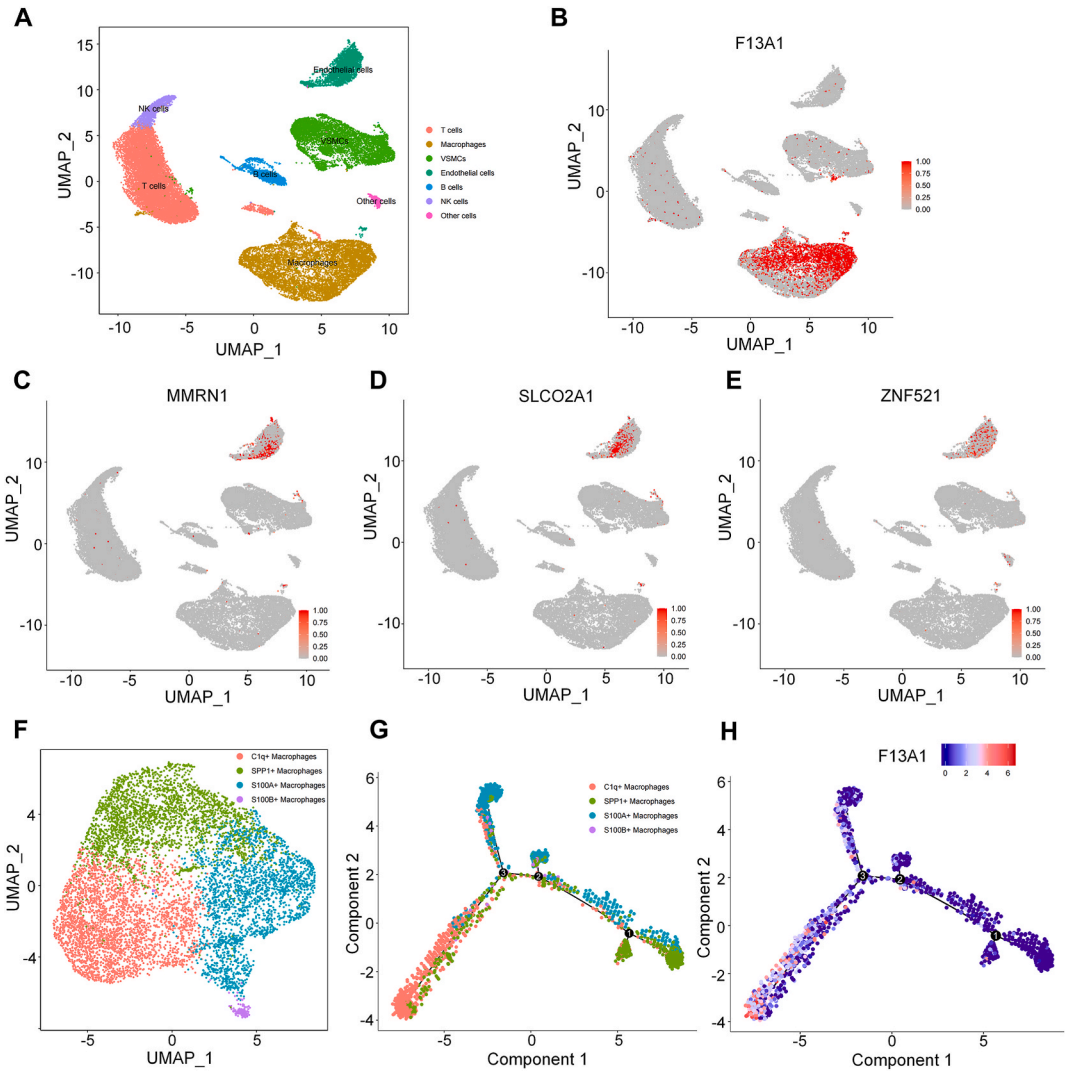

Fig. 11. Single-cell RNA sequencing analysis. (A) Dot map exhibits the main UMAP dimensionality reduction clustering and cell types of each clustering. (B–E) The high expression location of each hub genes in each type of cells in AS plaque. (F) Dotmap of the main UMAP dimensionality reduction clustering exhibits the subtypes of macrophages. (G) Dot map exhibits the pseudotime analysis result of each subtype of macrophages. (H) Dot map shows the main distribution and expression level of F13A1 in pseudotime analysis result.

pivotal biomarkers for the diagnose of AS progression in peripheral blood of MS patients, as well as found F13A1 as a potential macrophage differentiation regulator. Our study still remains some limitations. Firstly, although we combined multiple datasets to reduce bias, the sample size is still limited and it may affect the accuracy of the prediction model, while further validation with a larger datasets and clinical cohorts study in the future is needed. Secondly, since we used datasets from public databases, we could not ensure the quality of samples and the integrity of clinical data, which may cause potential biases. Additionally, due to the bioinformatic analysis and predictions without experimental validation, the function, mechanism, diagnostic value and potential therapeutic implications of F13A1 and other 3 hub genes in both AS progression of MS patients and immune system need to be excaveted and verified in further clinical cohorts and experimental study.

5. Conclusions

Our study has undertaken a systematic exploration, revealing 4 immune-associated hub genes (F13A1, MMRN1, SLCO2A1 and ZNF521). We constructed a nomogram to facilitate the diagnosis of AS in the presence of MS, and underscored immune cell dysregulation within AS plaques through extensive bioinformatics analysis and machine learning algorithms. Single-cell analysis identified F13A1 as a potential regulator of macrophage differentiation in AS plaque processing. Furthermore, we delved into miRNA and lncRNA predictions and drug-protein interaction, which offering promising avenues for potential preventive measures against AS progression in individuals with MS. With our findings, these hub genes may emerge as potential diagnostic and therapeutic targets

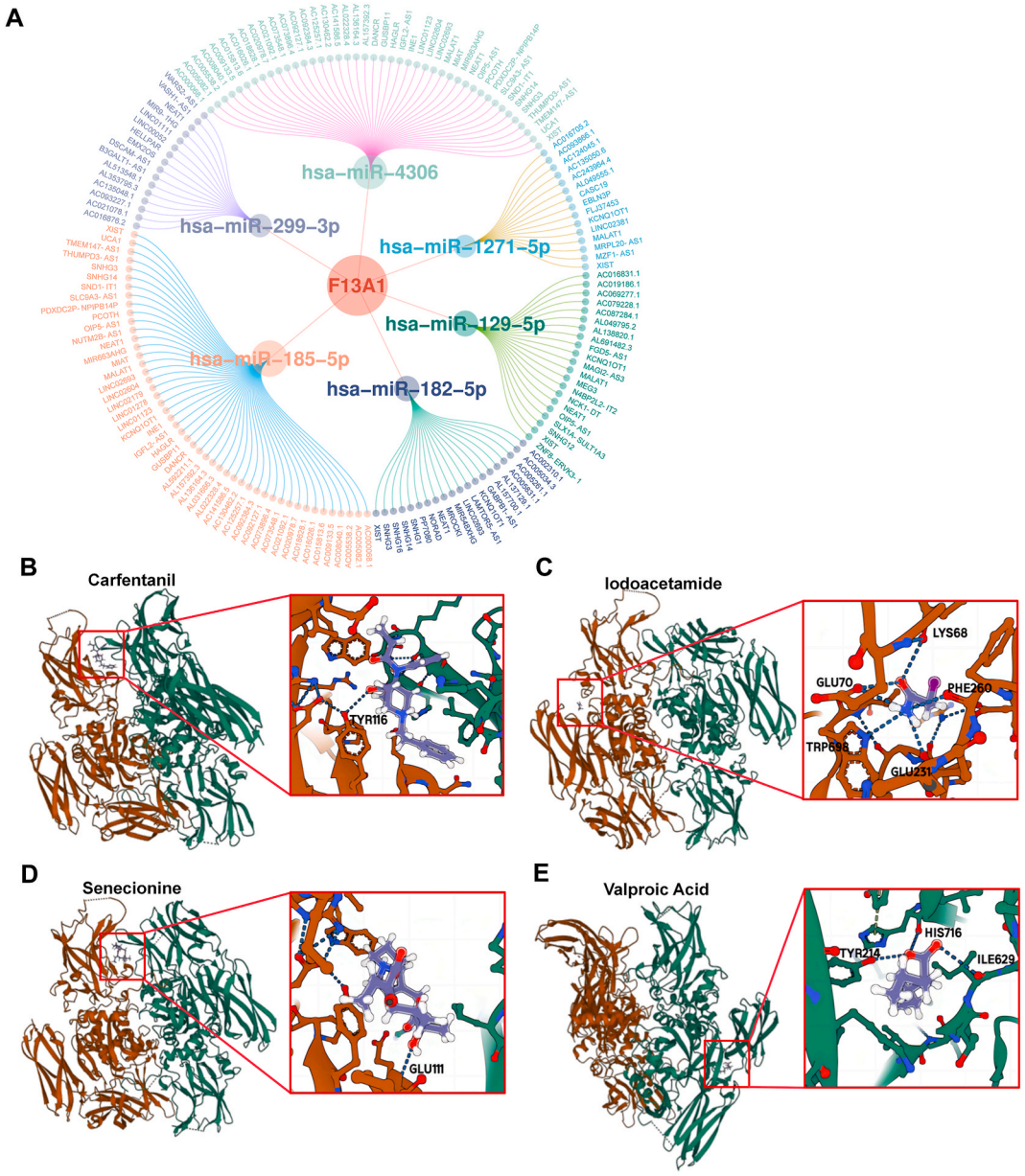

Fig. 12. The ceRNA network and the binding modes of screened drugs to F13A1. (A) The outer circles indicate the 164 predicted lncRNAs, inner circles indicate the 6 predicted miRNAs and the interaction relationship with F13A1. All lines indicate the interaction edge. (B) Binding mode of Carfentanil to F13A1 with binding energy of −7.906 kcal/mol. (C) Binding mode of Iodoacetamide to F13A1 with binding energy of −3.556 kcal/mol. (D) Binding mode of Senecionine to F13A1 with binding energy of −7.836 kcal/mol. (E) Binding mode of Valproic Acid to F13A1 with binding energy of −4.795 kcal/mol.

within the peripheral blood context for managing AS progression in MS patients.

Data availability statement

The datasets presented in this study can be found in online repositories. The names of the repositories and accession numbers can be found in the article/Supplementary Material.

CRediT authorship contribution statement

Da-Sheng Ning: Writing – review & editing, Writing – original draft, Software, Methodology. **Zi-Qing Zhou:** Investigation, Formal

analysis, Software. **Shu-Heng Zhou:** Resources, Formal analysis. **Ji-Mei Chen:** Supervision, Project administration, Funding acquisition.

Declaration of competing interest

The authors declare that they have no known competing financial interests or personal relationships that could have appeared to influence the work reported in this paper.

Acknowledgments

This study was supported by Medical Scientific Research Foundation of Guangdong Province(A2024373), National Key R&D Program of China(No. 2022YFC2407406), Science and Technology Fundation for Guangzhou Health(No:2023A031004), Guangzhou Science and Technology Planning Project(2023B03J0596) and Guangdong Peak Project(No. DFJH2020029).

Appendix A. Supplementary data

Supplementary data to this article can be found online at https://doi.org/10.1016/j.heliyon.2024.e34295.

References

[1] M. Back, A. Yurdagul Jr., I. Tabas, K. Oorni, P.T. Kovanen, Inflammation and its resolution in atherosclerosis: mediators and therapeutic opportunities, Nat. Rev. Cardiol. 16 (2019) 389–406.
[2] W.C. Keeter, S. Ma, N. Stahr, A.K. Moriarty, E.V. Galkina, Atherosclerosis and multi-organ-associated pathologies, Semin. Immunopathol. 44 (2022) 363–374.
[3] K. Kobiyama, K. Ley, Atherosclerosis, Circ. Res. 123 (2018) 1118–1120.
[4] Y.S. Liu, Q.J. Wu, Y. Xia, J.Y. Zhang, Y.T. Jiang, Q. Chang, Y.H. Zhao, Carbohydrate intake and risk of metabolic syndrome: a dose-response meta-analysis of observational studies, Nutr. Metabol. Cardiovasc. Dis. 29 (2019) 1288–1298.
[5] E. McCracken, M. Monaghan, S. Sreenivasan, Pathophysiology of the metabolic syndrome, Clin. Dermatol. 36 (2018) 14–20.
[6] J. Myers, P. Kokkinos, E. Nyelin, Physical activity, Cardiorespiratory fitness, and the metabolic syndrome, Nutrients 11 (2019).
[7] J. Wittwer, D. Bradley, Clusterin and its role in insulin resistance and the cardiometabolic syndrome, Front. Immunol. 12 (2021) 612496.
[8] J.L. Silveira Rossi, S.M. Barbalho, R. Reverete de Araujo, M.D. Bechara, K.P. Sloan, L.A. Sloan, Metabolic syndrome and cardiovascular diseases: going beyond traditional risk factors, Diabetes Metab Res Rev 38 (2022) e3502.
[9] F. Juul, G. Vaidean, N. Parekh, Ultra-processed foods and cardiovascular diseases: potential mechanisms of action, Adv. Nutr. 12 (2021) 1673–1680.
[10] R. Parsanathan, S.K. Jain, Novel invasive and noninvasive cardiac-specific biomarkers in obesity and cardiovascular diseases, Metab. Syndr. Relat. Disord. 18 (2020) 10–30.
[11] P. Libby, The changing landscape of atherosclerosis, Nature 592 (2021) 524–533.
[12] T. Barrett, S.E. Wilhite, P. Ledoux, C. Evangelista, I.F. Kim, M. Tomashevsky, K.A. Marshall, K.H. Phillippy, P.M. Sherman, M. Holko, A. Yefanov, H. Lee, N. Zhang, C.L. Robertson, N. Serova, S. Davis, A. Soboleva, NCBI GEO: archive for functional genomics data sets–update, Nucleic Acids Res. 41 (2013) D991–D995.
[13] M. Kanehisa, S. Goto, KEGG: kyoto encyclopedia of genes and genomes, Nucleic Acids Res. 28 (2000) 27–30.
[14] C. The Gene Ontology, The gene Ontology resource: 20 years and still GOing strong, Nucleic Acids Res. 47 (2019) D330–D338.
[15] K. Ellis, J. Kerr, S. Godbole, G. Lanckriet, D. Wing, S. Marshall, A random forest classifier for the prediction of energy expenditure and type of physical activity from wrist and hip accelerometers, Physiol. Meas. 35 (2014) 2191–2203.
[16] C. Yang, C. Delcher, E. Shenkman, S. Ranka, Machine learning approaches for predicting high cost high need patient expenditures in health care, Biomed. Eng. Online 17 (2018) 131.
[17] D. Szklarczyk, A.L. Gable, K.C. Nastou, D. Lyon, R. Kirsch, S. Pyysalo, N.T. Doncheva, M. Legeay, T. Fang, P. Bork, L.J. Jensen, C. von Mering, The STRING database in 2021: customizable protein-protein networks, and functional characterization of user-uploaded gene/measurement sets, Nucleic Acids Res. 49 (2021) D605–D612.
[18] A.M. Newman, C.L. Liu, M.R. Green, A.J. Gentles, W. Feng, Y. Xu, C.D. Hoang, M. Diehn, A.A. Alizadeh, Robust enumeration of cell subsets from tissue expression profiles, Nat. Methods 12 (2015) 453–457.
[19] M.D. Wilkerson, D.N. Hayes, ConsensusClusterPlus: a class discovery tool with confidence assessments and item tracking, Bioinformatics 26 (2010) 1572–1573.
[20] S.A. Wani, S.A. Khan, S.M.K. Quadri, scJVAE: a novel method for integrative analysis of multimodal single-cell data, Comput. Biol. Med. 158 (2023) 106865.
[21] T. Wu, E. Hu, S. Xu, M. Chen, P. Guo, Z. Dai, T. Feng, L. Zhou, W. Tang, L. Zhan, X. Fu, S. Liu, X. Bo, G. Yu, clusterProfiler 4.0: a universal enrichment tool for interpreting omics data, Innovation 2 (2021) 100141.
[22] J.H. Li, S. Liu, H. Zhou, L.H. Qu, J.H. Yang, starBase v2.0: decoding miRNA-ceRNA, miRNA-ncRNA and protein-RNA interaction networks from large-scale CLIP-Seq data, Nucleic Acids Res. 42 (2014) D92–D97.
[23] G.M. Morris, R. Huey, A.J. Olson, Using AutoDock for ligand-receptor docking, Curr Protoc, Bioinformatics (2008) (Chapter 8) Unit 24 (1) 8.14.1–8.14.40.
[24] A. Devesa, M. Lobo-Gonzalez, J. Martinez-Milla, B. Oliva, I. Garcia-Lunar, A. Mastrangelo, S. Espana, J. Sanz, J.M. Mendiguren, H. Bueno, J.J. Fuster, V. Andres, A. Fernandez-Ortiz, D. Sancho, L. Fernandez-Friera, J. Sanchez-Gonzalez, X. Rossello, B. Ibanez, V. Fuster, Bone marrow activation in response to metabolic syndrome and early atherosclerosis, Eur. Heart J. 43 (2022) 1809–1828.
[25] D.S. Ning, J. Ma, Y.M. Peng, Y. Li, Y.T. Chen, S.X. Li, Z. Liu, Y.Q. Li, Y.X. Zhang, Y.P. Jian, Z.J. Ou, J.S. Ou, Apolipoprotein A-I mimetic peptide inhibits atherosclerosis by increasing tetrahydrobiopterin via regulation of GTP-cyclohydrolase 1 and reducing uncoupled endothelial nitric oxide synthase activity, Atherosclerosis 328 (2021) 83–91.
[26] A.R. Tall, D.G. Thomas, A.G. Gonzalez-Cabodevilla, I.J. Goldberg, Addressing dyslipidemic risk beyond LDL-cholesterol, J. Clin. Invest. 132 (2022).
[27] S.K. Wculek, G. Dunphy, I. Heras-Murillo, A. Mastrangelo, D. Sancho, Metabolism of tissue macrophages in homeostasis and pathology, Cell. Mol. Immunol. 19 (2022) 384–408.
[28] M. Yamaoka-Tojo, T. Tojo, K. Wakaume, R. Kameda, S. Nemoto, N. Takahira, T. Masuda, T. Izumi, Circulating interleukin-18: a specific biomarker for atherosclerosis-prone patients with metabolic syndrome, Nutr. Metab. 8 (2011) 3.
[29] T. Xia, G. Chen, D. Zhou, W. Liu, X. Li, H. Gu, Y. Ye, J. Du, J. Fan, X. Peng, Nucleic acid probe-based difunctional hematology analysis kit for peripheral blood cell analysis, ACS Sens. 7 (2022) 469–476.

[30] F. Adam, S. Zheng, N. Joshi, D.S. Kelton, A. Sandhu, Y. Suehiro, S.B. Jeimy, A.V. Santos, J.M. Masse, J.G. Kelton, E.M. Cramer, C.P. Hayward, Analyses of cellular multimerin 1 receptors: in vitro evidence of binding mediated by alphaIIbbeta3 and alphavbeta3, Thromb. Haemostasis 94 (2005) 1004–1011.
[31] A. Leatherdale, D. Parker, S. Tasneem, Y. Wang, D. Bihan, A. Bonna, S.W. Hamaia, P.L. Gross, H. Ni, B.W. Doble, D. Lillicrap, R.W. Farndale, C.P.M. Hayward, Multimerin 1 supports platelet function in vivo and binds to specific GPAGPOGPX motifs in fibrillar collagens that enhance platelet adhesion, J. Thromb. Haemostasis 19 (2021) 547–561.
[32] D.N. Parker, S. Tasneem, R.W. Farndale, D. Bihan, J.E. Sadler, S. Sebastian, P.G. de Groot, C.P. Hayward, The functions of the A1A2A3 domains in von Willebrand factor include multimerin 1 binding, Thromb. Haemostasis 116 (2016) 87–95.
[33] S. Tasneem, F. Adam, I. Minullina, M. Pawlikowska, S.K. Hui, S. Zheng, J.L. Miller, C.P. Hayward, Platelet adhesion to multimerin 1 in vitro: influences of platelet membrane receptors, von Willebrand factor and shear, J. Thromb. Haemostasis 7 (2009) 685–692.
[34] J. Zhou, Y.S. Li, S. Chien, Shear stress-initiated signaling and its regulation of endothelial function, Arterioscler. Thromb. Vasc. Biol. 34 (2014) 2191–2198.
[35] M. Zhou, Y. Yu, R. Chen, X. Liu, Y. Hu, Z. Ma, L. Gao, W. Jian, L. Wang, Wall shear stress and its role in atherosclerosis, Front Cardiovasc Med 10 (2023) 1083547.
[36] P. Roy, M. Orecchioni, K. Ley, How the immune system shapes atherosclerosis: roles of innate and adaptive immunity, Nat. Rev. Immunol. 22 (2022) 251–265.
[37] C. Combadiere, S. Potteaux, M. Rodero, T. Simon, A. Pezard, B. Esposito, R. Merval, A. Proudfoot, A. Tedgui, Z. Mallat, Combined inhibition of CCL2, CX3CR1, and CCR5 abrogates Ly6C(hi) and Ly6C(lo) monocytosis and almost abolishes atherosclerosis in hypercholesterolemic mice, Circulation 117 (2008) 1649–1657.
[38] K.J. Moore, F.J. Sheedy, E.A. Fisher, Macrophages in atherosclerosis: a dynamic balance, Nat. Rev. Immunol. 13 (2013) 709–721.
[39] F. Tacke, D. Alvarez, T.J. Kaplan, C. Jakubzick, R. Spanbroek, J. Llodra, A. Garin, J. Liu, M. Mack, N. van Rooijen, S.A. Lira, A.J. Habenicht, G.J. Randolph, Monocyte subsets differentially employ CCR2, CCR5, and CX3CR1 to accumulate within atherosclerotic plaques, J. Clin. Invest. 117 (2007) 185–194.
[40] I. Tabas, A.H. Lichtman, Monocyte-Macrophages and T Cells in atherosclerosis, Immunity 47 (2017) 621–634.
[41] A. Shapouri-Moghaddam, S. Mohammadian, H. Vazini, M. Taghadosi, S.A. Esmaeili, F. Mardani, B. Seifi, A. Mohammadi, J.T. Afshari, A. Sahebkar, Macrophage plasticity, polarization, and function in health and disease, J. Cell. Physiol. 233 (2018) 6425–6440.
[42] Y. Wang, K. Yan, J. Lin, J. Li, J. Bi, Macrophage M2 Co-expression factors correlate with the immune microenvironment and predict outcome of renal clear cell carcinoma, Front. Genet. 12 (2021) 615655.
[43] J.L. Witztum, A.H. Lichtman, The influence of innate and adaptive immune responses on atherosclerosis, Annu. Rev. Pathol. 9 (2014) 73–102.
[44] T. Nakanishi, Y. Ohno, R. Aotani, S. Maruyama, H. Shimada, S. Kamo, H. Oshima, M. Oshima, J.D. Schuetz, I. Tamai, A novel role for OATP2A1/SLCO2A1 in a murine model of colon cancer, Sci. Rep. 7 (2017) 16567.
[45] T. Nakanishi, Y. Nakamura, J. Umeno, Recent advances in studies of SLCO2A1 as a key regulator of the delivery of prostaglandins to their sites of action, Pharmacol. Ther. 223 (2021) 107803.
[46] J. Umeno, T. Hisamatsu, M. Esaki, A. Hirano, N. Kubokura, K. Asano, S. Kochi, S. Yanai, Y. Fuyuno, K. Shimamura, N. Hosoe, H. Ogata, T. Watanabe, K. Aoyagi, H. Ooi, K. Watanabe, S. Yasukawa, F. Hirai, T. Matsui, M. Iida, T. Yao, T. Hibi, K. Kosaki, T. Kanai, T. Kitazono, T. Matsumoto, A hereditary enteropathy caused by mutations in the SLCO2A1 gene, encoding a prostaglandin transporter, PLoS Genet. 11 (2015) e1005581.
[47] Z. Zhang, W. Xia, J. He, Z. Zhang, Y. Ke, H. Yue, C. Wang, H. Zhang, J. Gu, W. Hu, W. Fu, Y. Hu, M. Li, Y. Liu, Exome sequencing identifies SLCO2A1 mutations as a cause of primary hypertrophic osteoarthropathy, Am. J. Hum. Genet. 90 (2012) 125–132.
[48] M.M. Syeda, X. Jing, R.H. Mirza, H. Yu, R.S. Sellers, Y. Chi, Prostaglandin transporter modulates wound healing in diabetes by regulating prostaglandin-induced angiogenesis, Am. J. Pathol. 181 (2012) 334–346.
[49] D. Wolf, K. Ley, Immunity and inflammation in atherosclerosis, Circ. Res. 124 (2019) 315–327.
[50] I. Hilgendorf, I. Theurl, L.M. Gerhardt, C.S. Robbins, G.F. Weber, A. Gonen, Y. Iwamoto, N. Degousee, T.A. Holderried, C. Winter, A. Zirlik, H.Y. Lin, G. K. Sukhova, J. Butany, B.B. Rubin, J.L. Witztum, P. Libby, M. Nahrendorf, R. Weissleder, F.K. Swirski, Innate response activator B cells aggravate atherosclerosis by stimulating T helper-1 adaptive immunity, Circulation 129 (2014) 1677–1687.
[51] A.P. Sage, M. Nus, L.L. Baker, A.J. Finigan, L.M. Masters, Z. Mallat, Regulatory B cell-specific interleukin-10 is dispensable for atherosclerosis development in mice, Arterioscler. Thromb. Vasc. Biol. 35 (2015) 1770–1773.
[52] A.C. Strom, A.J. Cross, J.E. Cole, P.A. Blair, C. Leib, M.E. Goddard, E.C. Rosser, I. Park, A. Hultgardh Nilsson, J. Nilsson, C. Mauri, C. Monaco, B regulatory cells are increased in hypercholesterolaemic mice and protect from lesion development via IL-10, Thromb. Haemostasis 114 (2015) 835–847.
[53] B.S. Garrison, A.P. Rybak, I. Beerman, B. Heesters, F.E. Mercier, D.T. Scadden, D. Bryder, R. Baron, D.J. Rossi, ZFP521 regulates murine hematopoietic stem cell function and facilitates MLL-AF9 leukemogenesis in mouse and human cells, Blood 130 (2017) 619–624.
[54] T. Hiratsuka, Y. Takei, R. Ohmori, Y. Imai, M. Ozeki, K. Tamaki, H. Haga, T. Nakamura, T. Tsuruyama, ZFP521 contributes to pre-B-cell lymphomagenesis through modulation of the pre-B-cell receptor signaling pathway, Oncogene 35 (2016) 3227–3238.
[55] P. Srikakulapu, C.A. McNamara, B cells and atherosclerosis, Am. J. Physiol. Heart Circ. Physiol. 312 (2017) H1060–H1067.
[56] K.Y. Tseng, S. Lin, Zinc finger factor 521 enhances adipogenic differentiation of mouse multipotent cells and human bone marrow mesenchymal stem cells, Oncotarget 6 (2015) 14874–14884.
[57] C. Soendergaard, P.H. Kvist, J.B. Seidelin, O.H. Nielsen, Tissue-regenerating functions of coagulation factor XIII, J. Thromb. Haemostasis 11 (2013) 806–816.
[58] Y. Maekawa, T. Nogita, M. Yamada, Favorable effects of plasma factor XIII on lower esophageal sphincter pressure of progressive systemic sclerosis, Arch. Dermatol. 123 (1987) 1440–1441.
[59] J. Thivolet, H. Perrot, F. Meunier, B. Bouchet, [Therapeutic action of coagulation factor XIII in scleroderma. 20 cases], Nouv. Presse Med. 4 (1975) 2779–2782.
[60] J.E. Nor, R.S. Mitra, M.M. Sutorik, D.J. Mooney, V.P. Castle, P.J. Polverini, Thrombospondin-1 induces endothelial cell apoptosis and inhibits angiogenesis by activating the caspase death pathway, J. Vasc. Res. 37 (2000) 209–218.
[61] F. De Paoli, J. Eeckhoute, C. Copin, J. Vanhoutte, C. Duhem, B. Derudas, J. Dubois-Chevalier, S. Colin, C. Zawadzki, B. Jude, S. Haulon, P. Lefebvre, B. Staels, G. Chinetti-Gbaguidi, The neuron-derived orphan receptor 1 (NOR1) is induced upon human alternative macrophage polarization and stimulates the expression of markers of the M2 phenotype, Atherosclerosis 241 (2015) 18–26.
[62] M.T. Kaartinen, M. Arora, S. Heinonen, A. Rissanen, J. Kaprio, K.H. Pietilainen, Transglutaminases and obesity in humans: association of F13A1 to adipocyte hypertrophy and adipose tissue immune response, Int. J. Mol. Sci. 21 (2020).
[63] E. Galkina, K. Ley, Immune and inflammatory mechanisms of atherosclerosis (*), Annu. Rev. Immunol. 27 (2009) 165–197.
[64] A. Sarvary, S. Szucs, I. Balogh, A. Becsky, H. Bardos, M. Kavai, U. Seligsohn, R. Egbring, S. Lopaciuk, L. Muszbek, R. Adany, Possible role of factor XIII subunit A in Fcgamma and complement receptor-mediated phagocytosis, Cell. Immunol. 228 (2004) 81–90.
[65] M. Naito, H. Nomura, A. Iguchi, W.D. Thompson, E.B. Smith, Effect of crosslinking by factor XIIIa on the migration of vascular smooth muscle cells into fibrin gels, Thromb. Res. 90 (1998) 111–116.
[66] M. Son, A. Porat, M. He, J. Suurmond, F. Santiago-Schwarz, U. Andersson, T.R. Coleman, B.T. Volpe, K.J. Tracey, Y. Al-Abed, B. Diamond, C1q and HMGB1 reciprocally regulate human macrophage polarization, Blood 128 (2016) 2218–2228.
[67] M.S. Leisegang, LET's sponge: how the lncRNA PFL promotes cardiac fibrosis, Theranostics 8 (2018) 874–877.
[68] Z.M. Ye, S. Yang, Y.P. Xia, R.T. Hu, S. Chen, B.W. Li, S.L. Chen, X.Y. Luo, L. Mao, Y. Li, H. Jin, C. Qin, B. Hu, LncRNA MIAT sponges miR-149-5p to inhibit efferocytosis in advanced atherosclerosis through CD47 upregulation, Cell Death Dis. 10 (2019) 138.
[69] C. Yu, L. Li, F. Xie, S. Guo, F. Liu, N. Dong, Y. Wang, LncRNA TUG1 sponges miR-204-5p to promote osteoblast differentiation through upregulating Runx2 in aortic valve calcification, Cardiovasc. Res. 114 (2018) 168–179.
[70] X. Yang, H. Wang, H.M. Ni, A. Xiong, Z. Wang, H. Sesaki, W.X. Ding, L. Yang, Inhibition of Drp1 protects against senecionine-induced mitochondria-mediated apoptosis in primary hepatocytes and in mice, Redox Biol. 12 (2017) 264–273.
[71] K.C. Ricart, S. Bolisetty, M.S. Johnson, J. Perez, A. Agarwal, M.P. Murphy, A. Landar, The permissive role of mitochondria in the induction of haem oxygenase-1 in endothelial cells, Biochem. J. 419 (2009) 427–436.
[72] H. Lee, Y.J. Hwang, J.H. Park, D.H. Cho, Valproic acid decreases vascular smooth muscle cell proliferation via protein phosphatase 2A-mediated p70 S6 kinase inhibition, Biochem. Biophys. Res. Commun. 606 (2022) 94–99.